J. Fluid Mech. (1975), *vol.* 68, *part* 4, *pp.* 639–672
Printed in Great Britain

Experiments on turbulence in a rotating fluid

By A. IBBETSON
Department of Geophysics, University of Reading, England
AND D. J. TRITTON
Department of Geophysics and Planetary Physics, School of Physics, University of Newcastle upon Tyne, England

(Received 6 July 1974)

Experiments have been carried out to investigate the effect of rotation of the whole system on decaying turbulence, generally similar to grid turbulence, generated in air in an annular container on a rotating table. Measurements to determine the structure of the turbulence were made during its decay, mean quantities being determined by a mixture of time and ensemble averaging. Quantities measured (as functions of time after the turbulence generation) were turbulence intensities perpendicular to and parallel to the rotation axis, spectra of these two components with respect to a wavenumber perpendicular to the rotation axis, and some correlation coefficients, selected to detect differences in length scales perpendicular and parallel to the rotation axis. The intensity measurements were made for a wide range of rotation rates; the other measurements were made at a single rotation rate (selected to give a Rossby number varying during the decay from about 1 to small values) and, for comparison, at zero rotation. Subsidiary experiments were carried out to measure the spin-up time of the system, and to determine whether the turbulence produced any mean flow relative to the container.

A principal result is that increasing the rotation rate produces faster decay of the turbulence; the nature of the additional energy sink is an important part of the interpretation. Other features of the results are as follows: the measurements without rotation can be satisfactorily related to wind-tunnel measurements; even with rotation, the ratio of the intensities in the two directions remains substantially constant; the normalized spectra for the rotating and the non-rotating cases show surprising similarity but do contain slight systematic differences, consistent with the length scales indicated by the correlations; rotation produces a large increase in the length scale parallel to the rotation axis and a smaller increase in that perpendicular to it; the turbulence produces no measurable mean flow.

A model for the interpretation of the results is developed in terms of the action of inertial waves in carrying energy to the boundaries of the enclosure, where it is dissipated in viscous boundary layers. The model provides satisfactory explanations of the overall decay of the turbulence and of the decay of individual spectral components. Transfer of energy between wavenumbers plays a much less significant role in the dynamics of decay than in a non-rotating fluid. The relationship of the model to the interpretation of the length-scale difference in terms of the Taylor–Proudman theorem is discussed.

The model implies that the overall dimensions of the system enter in an important way into the dynamics. This imposes a serious limitation on the application of the results to the geophysical situations at which experiments of this type are aimed.

The paper includes some discussion of the possibility of energy transfer from the turbulence to a mean motion (the 'vorticity expulsion' hypothesis). It is possible, on the basis of the observations, to exclude this process as the additional turbulence energy sink. But this does not provide any evidence either for or against the hypothesis in the conditions for which it has been postulated.

1. Introduction

The importance for a variety of geophysical and other applications of gaining an understanding of the basic dynamics of turbulent motion in a rotating fluid is sufficiently apparent that we need not dwell on it here. All experience of turbulence studies in non-rotating fluids suggests that such an understanding will not be achieved without a body of experimental data. However, it is by no means obvious at the outset just what experiments should be done, or perhaps more significantly, just what experiments can be done. The first stage must consist of general exploratory experiments. This paper describes an attempt to find a point of entry into the problem. Our work perhaps asks as many questions as it answers, but we believe that one begins to know the right questions to ask only after some data have been accumulated.

The point of view behind our experiments was as follows. Experiments on decaying turbulence behind a grid in a wind tunnel have been a fruitful source of ideas extending far beyond their immediate context. A corresponding experiment in a rotating fluid might be similarly seminal. In principle, therefore, one would like to put the wind tunnel on a rotating turntable. In practice the limitations on what can be achieved in this way are very severe. In fact quantitative design considerations forced us to reject, very reluctantly, any arrangement involving the usual space–time transformation for observing the decay. We shall not recount these considerations here in any detail, but the essential points are the following. One requires the Reynolds number of the turbulence to be large and the Rossby number to extend to small values, so that the motion is fully turbulent but may be strongly affected by the rotation. Both these indicate the use of a large length scale. However, as discussed below, we wished to observe all stages of the decay; this can be done in a wind tunnel, even in a non-rotating fluid, only by making the length scale small (Batchelor & Townsend 1948*b*).

Before describing the method used to circumvent this problem, it should be mentioned that a rotating wind-tunnel experiment has been performed by Traugott (1958). His results are of some interest, but he was able to observe only the very early stages of the decay.

In our experiment the turbulence was generated in an enclosed tank of air on a rotating turntable. Its properties were then observed as functions of time. The principal disadvantage of this procedure is, of course, that one cannot use simple time averaging to determine mean quantities. Instead a combination of time and

ensemble averaging was used. In a single run, the signal from a probe being traversed through the fluid was averaged over a time interval short compared with the overall development time scale of the turbulence. A number of similar runs was performed, and further averaging carried out over the results for corresponding stages of development of the turbulence from different runs.

The experimental arrangement, of which further details will be given in § 2, is not necessarily to be expected to generate turbulence of exactly the same properties (e.g. degree of isotropy, length scale in relation to generating grid length scale, etc.) as a grid in a wind tunnel. However, our experiment consists essentially of a direct comparison of the properties and behaviour of the turbulence with and without rotation of the tank. The changes due to rotation may thus be studied even if the non-rotating turbulent motion is incompletely specified. Also, even at the higher rotation rates, the process by which the turbulence is generated occurs at reasonably high Rossby number and should thus be little affected by the rotation. The Rossby number becomes smaller as the turbulence decays, and the effect of rotation becomes increasingly important. Thus the experiment essentially compares the development in rotating and in non-rotating fluid of turbulence that was initially similar in the two cases.

The quantities measured were all standard quantities of turbulence research. However, experimental expediency played a substantial role in deciding on the particular quantities to be measured.

Experiments of this type make the assumption that distant boundaries have little effect. In a rotating fluid this is a more questionable assumption than in a non-rotating fluid. In fact, if our interpretation of our observations is correct, this effect turns out to be the most serious limitation on the extrapolation from our laboratory experiments to geophysical situations.

Although the work was primarily exploratory in character, there was one obvious specific question to be answered by it: would the turbulence decay more rapidly or more slowly when the tank was rotating? *A priori*, simple but inconclusive arguments could be (and were) advanced for either answer. One could argue that rotation is essentially stabilizing, and should therefore suppress the turbulence, i.e. produce faster decay. (But this argument does not indicate where the energy removed from the turbulence reappears.) Conversely, one could argue that the effect of rotation would be to make the turbulence more nearly two-dimensional, thus suppressing the transfer of energy to higher wavenumbers; this would reduce the dissipation and so produce slower decay. At the start of our work this seemed to be an entirely open question, and it was the main reason for our wishing to be able to observe the decay process over a long time.

2. Apparatus and technical details

As has been outlined in § 1, the simultaneous requirements of large initial Reynolds number and ability to observe the decay until the Rossby number became small necessitated that the experiment should be done as a 'real-time' decay experiment, using ensemble averaging to accumulate statistical data. The

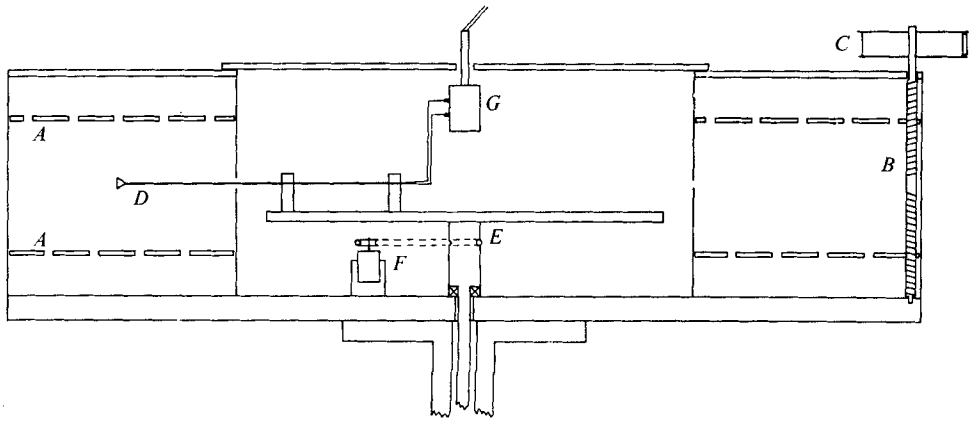

FIGURE 1. Schematic diagram of apparatus. Cross-section through the rotating annulus showing perforated grids *A* producing turbulence supported on three screwed rods *B* driven by three pulleys *C*. The hot-wire anemometer and streamlined support arm *D* are rotated with respect to the annulus on the inner turntable *E* driven by a motor *F*. Electrical signals from the hot wire are transmitted from the turntable via the low-noise slip-rings *G*.

apparatus was therefore required to produce large intensity turbulence in an enclosed volume of fluid, to do it reproducibly over large numbers of repeated experiments, and to do it while rotating at different speeds. The need to measure different turbulence velocity components indicated the use of air as the working fluid and hot wires for the measurements.

A diagram of the essential mechanical details of the apparatus is shown in figure 1. The working air was contained in a cylindrical annulus having metal inner and outer walls and a Perspex lid at the top. The annulus was mounted on a flat turntable which formed the base of the working region, and which could be rotated at steady speeds up to 10 rad s^{-1}, driven by a synchronous motor through a servo-controlled electromagnetic clutch. As a compromise between the opposing requirements of a large apparatus (so that the length scale of the turbulence could be large) and ease of handling, the annulus was of square cross-section, height 0·30 m, inner radius 0·30 m and outer radius 0·60 m. The use of an annular working region permitted the probe traversing gear to be mounted on the axis of the turntable, and the probe to enter the annulus through its inner wall rather than its outer wall, thus keeping disturbances to the working region to a minimum (see below).

The turbulent motion was produced inside the annular region by making a single rapid traverse of two flat metal plates ('grids') which had regular arrays of circular holes drilled in them. The grids were supported, one above the other, on three screwed rods in the annulus; the lower halves of the rods were oppositely threaded from the upper halves, so that rotation of the rods caused the upper grid to move up and the lower grid to move down. The motion of the grids was produced by a reversible electric motor connected by belts to all three screwed rods, and was controlled by microswitches actuated by the grids. The holes in each grid were of diameter 10 mm and were located at the corners of a 50 mm square mesh covering the whole area of the grid; the open-area ratio was thus about $\frac{1}{30}$.

The two arrays were staggered, a hole in the upper grid being vertically above the centre of a mesh square on the lower grid and vice versa. The edges of each grid plate were lined with foam rubber which rubbed against the walls of the annulus and so minimized the air flow through the gaps.

In an experimental run the turbulence was produced by starting with the grids together near the centre of the annulus and the air at rest relative to the tank, and then traversing the grids apart to the lid and the floor of the annulus respectively. Since the regions behind the grids were enclosed all the air was driven through the holes. The initial flow thus consisted of an array of staggered, oppositely directed, turbulent jets, which interacted to produce a turbulence field in a way similar to the interaction of the wakes behind a conventional wind-tunnel grid. The final rest position of each grid was within 5 mm of the top or bottom of the annulus, and was reproducible between runs to within about ± 2 mm. The maximum speed of the grids was 60 mm s^{-1}, and the time taken to traverse the grids from their initial position to their final rest position was 3·2 s, including acceleration and deceleration. The maximum jet velocity w_J (grid velocity divided by open-area ratio) was thus about 1·8 m s^{-1}, giving a jet Reynolds number based on this and the hole diameter d of about 1200. The measured initial r.m.s. turbulence intensity was about 110 mm s^{-1} (see §3.1), giving an initial turbulence Reynolds number $v_0' M/\nu$ of about 360.†

The most rapid rotation rate used was 6·4 rad s^{-1}. Hence the Rossby number $w_J/\Omega d$ of the jets ranged down to 28, and one may expect these to be little affected by the rotation. The initial turbulence Rossby number $v_0'/\Omega M$ was, however, as low as 0·3 for the fastest rotation.

Figure 2 (plate 1) shows a photograph of the apparatus. The grids are in their final positions, so the upper one may be seen just below the (almost invisible) Perspex lid.

Measurements of the turbulence were made using hot-wire anemometers which were inserted into the annular region through a gap in the inner wall at about the midlevel. The region was not, therefore, completely closed. The disturbance to the air in the annulus caused by the gap, which was 7 mm wide, was investigated and found to be significant only within a distance of about 30 mm of the gap; it was, in any case, small compared with the disturbance caused by the probe itself. Because there was no mean air motion with respect to the annulus it was necessary to move the hot-wire anemometers relative to it: this served the dual purpose of enabling the anemometers to operate in the forced convection regime and of permitting averaging of the turbulence velocities with respect to the azimuthal co-ordinate ϕ. Because of the difficulty of stopping and starting such a probe suddenly, it was swept continuously around the annulus at a fixed radius, height and speed, mounted on an inner independently rotating table. The supporting arm for the hot-wire probe was therefore carefully streamlined to reduce disturbances in the working region. Also, the rotation speed of the probe relative to the tank was limited to 1·5 rad s^{-1} so as to maintain laminar flow in the wake of the 2 mm thick supporting arm.

The rotating hot-wire probe was connected to the rest of the anemometer

† A list of symbols is given in the appendix.

circuitry through low-noise silver slip-rings. The electrical noise introduced by the slip-rings into velocity measurements was always at least one order of magnitude below the minimum signal produced by the anemometer.

The hot wires were typically 1 mm long and of 2·5 μm diameter platinum wire etched from Wollaston wire. Both azimuthal and vertical velocity components were measured using an X-wire in the ϕ, z plane. The orientation of each wire in the X-wire was measured to within $\pm 1°$, and the sensitivities of the two wires were typically matched to within better than $\pm 3\%$. The anemometers were operated at constant current and were electronically compensated at the probe speed for falling response at high frequencies. The anemometer output signals were processed using conventional analog methods built around operational amplifiers with true time integration and digital print-out. The bandwidth of the electronic circuit was 0·5 Hz–4 kHz, which at a probe speed of about 600 mm s^{-1} corresponds to wavelengths from 1·2 m to 0·15 mm. One-dimensional energy spectra were measured using a Bruel & Kjaer octave filter set for frequencies down to 16 Hz supplemented by three two-stage R–C filters (of somewhat inferior characteristics) of nominally half-octave bandwidth down to 1·4 Hz. Two-point velocity correlations were measured using an analog multiplier (which also served as the squarer in the intensity and spectral measurements) and integrator.

The background noise, i.e. the anemometer reading in nominally still air, corresponded typically to a velocity fluctuation of order 0·6 mm s^{-1}. This probably came from a variety of sources, of which mechanical vibration and the disturbance introduced by the probe itself were predominant. The lower level readings were corrected for this noise on the reasonable assumption that the signal and the noise were uncorrelated, i.e. the mean-square noise was subtracted from the mean-square measured signal. Data were discarded when this correction became more than half of the measured signal. Because the noise level and, more particularly, its spectral distribution varied with the rotation rate, the stage to which the decay could be observed before the signal-to-noise ratio became unacceptable varied considerably between experiments.

Hot-wire anemometers were calibrated *in situ* by holding the anemometer fixed with respect to the laboratory and rotating the annulus, allowing the air inside it to reach a steady speed before each measurement. The accuracy of calibration of anemometer velocity-fluctuation sensitivity was about $\pm 2\%$ for azimuthal velocities and $\pm 7\%$ for vertical velocities. The overall accuracy of measurement of the various electronic gain factors was about $\pm 2\%$ for intensity measurements and about $\pm 4\%$ for spectral measurements.

The turbulence intensity during a run decreased with time, and so the averaging used was a combined time and ensemble averaging. The hot-wire anemometer signals were processed and then sampled using an electronic gate for a period of 1 s in every 4 s. The gated signal was integrated over the 1 s period, and measured on a printing digital voltmeter. The experiment was then repeated under exactly similar conditions, and further information on the decaying turbulence was obtained at precisely the same intervals during the decay, so that a sequence of ten experiments gave ten sequences of values of, say, v' at intervals of 4 s. Corresponding values within each sequence were then averaged so as to

obtain ensemble averages. The choice of a 1 s averaging time is of course a compromise between the requirements of short averaging time (so that the turbulence can be considered to be statistically steady during the interval) and long averaging time (to reduce the variance of the mean value). It corresponds (owing to the motion of the probe) to an average over about 13 grid mesh lengths. The decay during the integration period probably introduces significant errors into the values for $v'(t)$ and $w'(t)$ only when t is less than about 10 s. In practice it was usually found that variances of measured quantities were sufficiently small after averaging over an ensemble of ten runs, although in some of the spectral measurements, in the interest of time economy, accuracy was sacrificed by reducing the number of runs in an ensemble to six. Typical standard deviations of mean quantities will be presented in §3.

Although buoyancy effects were observed to modify the results under certain conditions, no attempt was made to insulate the annulus or to control its temperature. Air temperatures inside the annulus were, however, monitored using small thermocouples, one 20 mm above the base and the other 20 mm below the lid. These measurements were not made with great precision, and were only taken to indicate the presence or absence of vertical temperature stratification. In fact turbulence measurements were usually discontinued when the indicated temperature difference between top and bottom exceeded 0·5° C at any time. This corresponds to a value of the Brunt–Väisälä angular frequency N of about 0·2 rad s^{-1}, which is small compared with the values of 2Ω in most of the rotating experiments.

3. Experimental results

3.1. *The decay of turbulent intensities*

The r.m.s. intensities of the azimuthal (v') and vertical (w') turbulent velocity components were measured as functions of the time t after generation of the turbulence, using the methods described in §2. A selection of the results obtained is shown in figure 3, for various speeds of rotation of the apparatus ranging from 0 to 6·4 rad s^{-1}. The results have not been normalized in any way in this diagram so as to avoid any possible bias in interpretation. The origin, $t = 0$, is taken (somewhat arbitrarily) as the time at which the grid motion starts.

Measurements of the intensities of the two components are subject to the errors of calibration mentioned in §2, i.e. $\pm 2\,\%$ estimated standard error in the anemometer's horizontal velocity sensitivity, $\pm 7\,\%$ estimated standard error in its vertical velocity sensitivity, and $\pm 2\,\%$ estimated standard error in the gain factors of the electronic equipment. In addition, the use of only ten experimental runs in each ensemble mean leads to an uncertainty in the ensemble mean values of about $\pm 11\,\%$ (range: 7–15 %). The overall estimated standard error in a single measurement of r.m.s. turbulent intensity is thus $\pm 6\,\%$ for v' and $\pm 9\,\%$ for w'. These standard errors must be applied to all points plotted in figure 3.

The azimuthal intensity may be expected to be typical of the intensity in any horizontal direction. The symmetry of the generation process should ensure that anisotropy of the initial turbulence in a horizontal plane is much smaller than

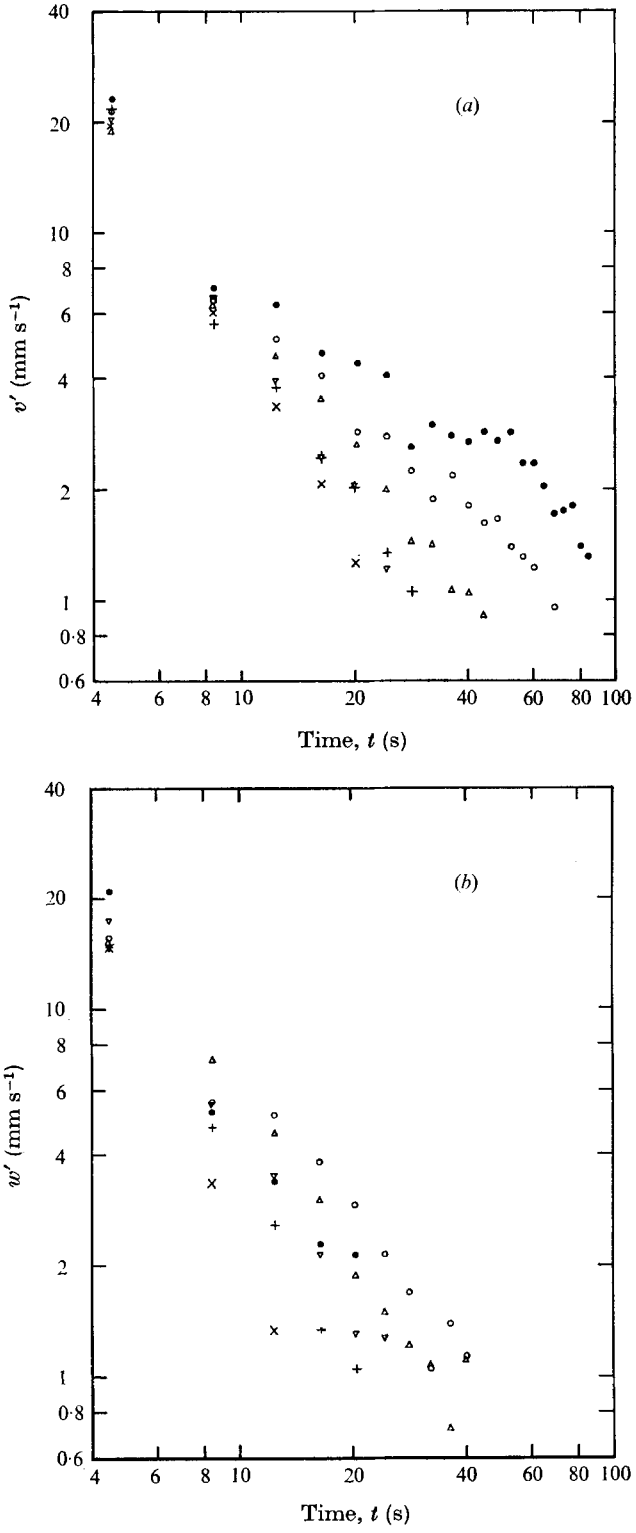

FIGURE 3. The decay of (*a*) the azimuthal component v' and (*b*) the vertical component w' of r.m.s. turbulence intensity with time t, for various rotation speeds Ω (rad s^{-1}). ●, $\Omega = 0$; ○, $\Omega = 1{\cdot}0$; △, $\Omega = 1{\cdot}6$; ▽, $\Omega = 2{\cdot}5$; +, $\Omega = 4{\cdot}0$; ×, $\Omega = 6{\cdot}4$.

Ω (rad s^{-1})	0	1·0	1·6	2·5	4·0	6·4
v_0' (mm s^{-1})	116	114	127	117	119	98
w_0' (mm s^{-1})	79	84	70	75	89	76
v_0'/w_0'	1·47	1·36	1·81	1·56	1·34	1·29

TABLE 1

that between vertical and horizontal components. The action of the Coriolis force on all horizontal components is similar and so the rotation is not to be expected to generate horizontal anisotropy, although its effect on the vertical component may be expected to be very different from that on the horizontal components. It would, of course, be desirable to check this supposition with some measurements of the radial intensity u'; this, however, has not yet been done, owing to the greater difficulty in using the appropriate form of X-wire in a way that does not disturb the motion.

The initial values (integrated from $t = 0$ to 1·0 s) of the azimuthal and vertical components of r.m.s. turbulence intensity, v_0' and w_0', together with their ratio are shown in table 1 as functions of the rotation speed Ω for one set of experiments. There is apparently no systematic variation of any of these quantities with increasing rotation speed. The intention (see §1) that the initial turbulence should be similar throughout, and that the effect of rotation should be seen only in the subsequent decay, appears to be fulfilled.

The subsequent decay of the turbulence, i.e. the interpretation of figure 3, will be discussed in §4.2.

Because of the labour involved, it has not been possible to measure quantities other than intensities for the same variety of rotation rates. On the basis of the intensity measurements, the case $\Omega = 2{\cdot}5\,\mathrm{rad\,s^{-1}}$ was selected for more detailed study. Figure 3 shows that, at this speed, the decay was being substantially affected by the rotation, but the initial conditions were fairly certainly little affected by it ($v_0'/\Omega M \simeq 1$). The more detailed measurements were also made at $\Omega = 0$ for comparison purposes.

3.2. *One-dimensional energy spectra*

Measurements of the energy spectra of the azimuthal and vertical velocity components were made as described in §2. It was assumed that a frequency–wavenumber transformation could be made using the probe's translation speed. The results are thus presented as one-dimensional spectra with respect to the wavenumber k_2 in the azimuthal direction.

Figures 4 (*a*)–(*e*) show the results for $\Omega = 0$ and $\Omega = 2{\cdot}5\,\mathrm{rad\,s^{-1}}$. The ordinate in each case is the spectral density $E(k_2)$ normalized with respect to the grid mesh length M and the energy of that particular velocity component at the corresponding stage of the decay. The total energies used in the normalization were determined from the spectral measurements themselves (from the area under the graph), and not from the measurements described in §3.1, to avoid possible systematic errors due to incomplete knowledge of the transfer functions of the

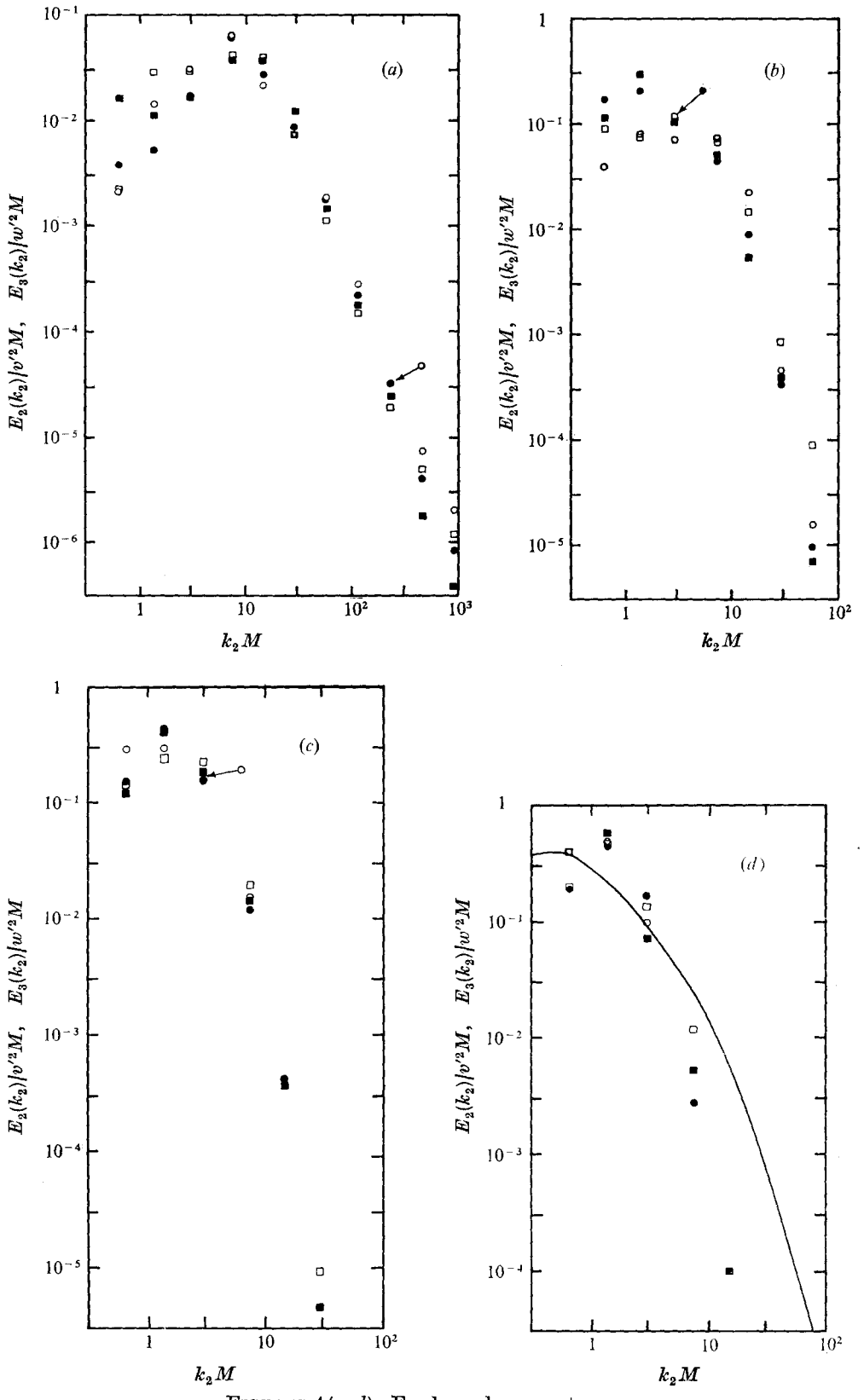

FIGURES 4(*a–d*). For legend see next page.

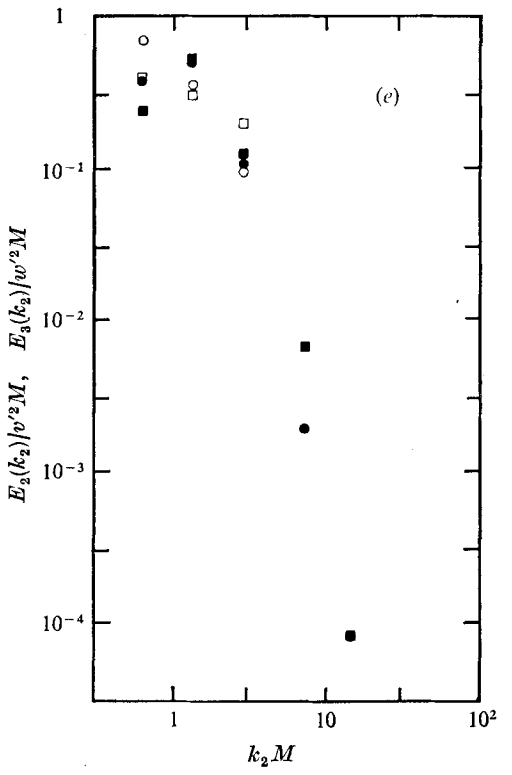

FIGURE 4. Normalized energy spectra $E_i(k_2)/u_i'^2M$ as functions of dimensionless wavenumber k_2M at different stages of the decay: (*a*) $t = 0{\cdot}5$ s; (*b*) $t = 4{\cdot}5$ s; (*c*) $t = 8{\cdot}5$ s; (*d*) $t = 12{\cdot}5$ s; (*e*) $t = 16{\cdot}5$ s. Spectra of azimuthal (v') and vertical (w') velocity components for both rotating ($\Omega = 2{\cdot}5$ rad s^{-1}) and non-rotating ($\Omega = 0$) experiments are plotted on each graph. ■, $\Omega = 0$, v'; □, $\Omega = 0$, w'; ●, $\Omega = 2{\cdot}5$, v'; ○, $\Omega = 2{\cdot}5$, w'. The line in (*d*) represents wind-tunnel data of Uberoi & Wallis (1969).

filters. (The agreement between total energies determined in the two ways is within the limits of experimental error except in the case of the vertical motion spectrum at $\Omega = 2{\cdot}5$ rad s^{-1}. In this case the total energies derived from the spectra are at all stages of the decay about 40 % smaller than the direct measurements. Hence the vertical motion spectra at $\Omega = 2{\cdot}5$ rad s^{-1} in figure 4 must be treated with some caution. The reason for the discrepancy is not known.)

The spectral measurements were again subject to the errors of calibration mentioned in § 3.1. However, the length of each experiment prohibited its repetition more than six times to form the ensemble mean. The standard error associated with the ensemble mean values is therefore about $\pm$ 18 % (range: 10–25 %). This leads to estimated standard errors in the spectra of $\pm$ 19 % for azimuthal velocities and $\pm$ 23 % for vertical velocities. These errors must be borne in mind when interpreting figures 4 (*a*)–(*e*).

Figure 4 (*d*) includes for comparison a wind-tunnel turbulence spectrum (Uberoi & Wallis 1969) at a corresponding stage of decay. The procedure for making the comparison will be explained, along with more general discussion of the spectral measurements, in § 4.3.

3.3. *Two-point velocity correlations*

For our system, spectral measurements are much more readily made than correlation measurements. However, because the spectra are necessarily measured with respect to the wavenumber k_2, they can give no indication of any anisotropy in the length scales. Since such anisotropy might well be a consequence of rotation, a few correlation measurements have been made, although the time required to do each experiment has restricted the measurements to only one value of the separation, namely 34 mm (the largest separation attainable in the vertical direction because of the initial positions of the grids). Moreover, only azimuthal velocity components were observed because of the difficulty of operating two X-wires simultaneously in the rotating annulus. The correlations measured were therefore $R_{22}(\Delta r = 34\,\mathrm{mm})$ and $R_{22}(\Delta z = 34\,\mathrm{mm})$ for the two cases $\Omega = 0$ and $2{\cdot}5\,\mathrm{rad\,s^{-1}}$. The four sets of measurements are thus directly comparable in the sense that in all cases the separation was perpendicular to the velocity component being measured (i.e., in conventional homogeneous turbulence notation, they are all g-type correlations).

The procedure used in evaluating correlations has been outlined in § 2. A second hot-wire probe was mounted on a second streamlined support arm, and adjusted so as to be 34 mm vertically above or radially displaced from the first probe. The probes were single vertical hot wires. Both probes were rotated at the same angular speed relative to the turntable inside the annulus. Signals from the anemometers were amplified, multiplied together, time integrated over an averaging period of 1 s, measured and printed out. During each run, values of the 1 s time-averaged covariances $\overline{v_a v_b}$ were averaged over, say, 12 experiments, and the covariance was normalized with respect to the geometrical mean of the intensities measured by probe (a) in 6 experiments and by probe (b) in 6 experiments. It was thus unnecessary to calibrate the anemometers at all.

The values of the correlations $R_{22}(\Delta r)$ and $R_{22}(\Delta z)$ as functions of the time t after the initiation of the turbulence at both $\Omega = 0$ and $\Omega = 2{\cdot}5\,\mathrm{rad\,s^{-1}}$ are shown in figure 5. Errors in the measurements are due mainly to the variance of the ensemble averages, and the spread of values at successive times may be taken as indicative of the accuracy achieved (typically $\pm 0{\cdot}1$). Obviously the errors are too large to allow very detailed comparison of the correlations, but it seems probable that after an initial settling-down period (say after $t = 10\,\mathrm{s}$) the correlations do not change very rapidly with time and are characterized by the following mean values ($10\,\mathrm{s} < t < 30\,\mathrm{s}$):

$$R_{22}(\Delta r) = 0{\cdot}34, \quad R_{22}(\Delta z) = 0{\cdot}30 \quad \text{at} \quad \Omega = 0,$$
$$R_{22}(\Delta r) = 0{\cdot}53, \quad R_{22}(\Delta z) = 0{\cdot}72 \quad \text{at} \quad \Omega = 2{\cdot}5.$$

3.4. *The spin-up time*

The interpretation of the measurements described above to be proposed in § 6 is related to the spin-up process, whereby steady motions relative to a rotating tank are damped out (Greenspan 1968, § 3.7). It is therefore useful to know the spin-up time for our apparatus. It has been shown that, if the boundaries are

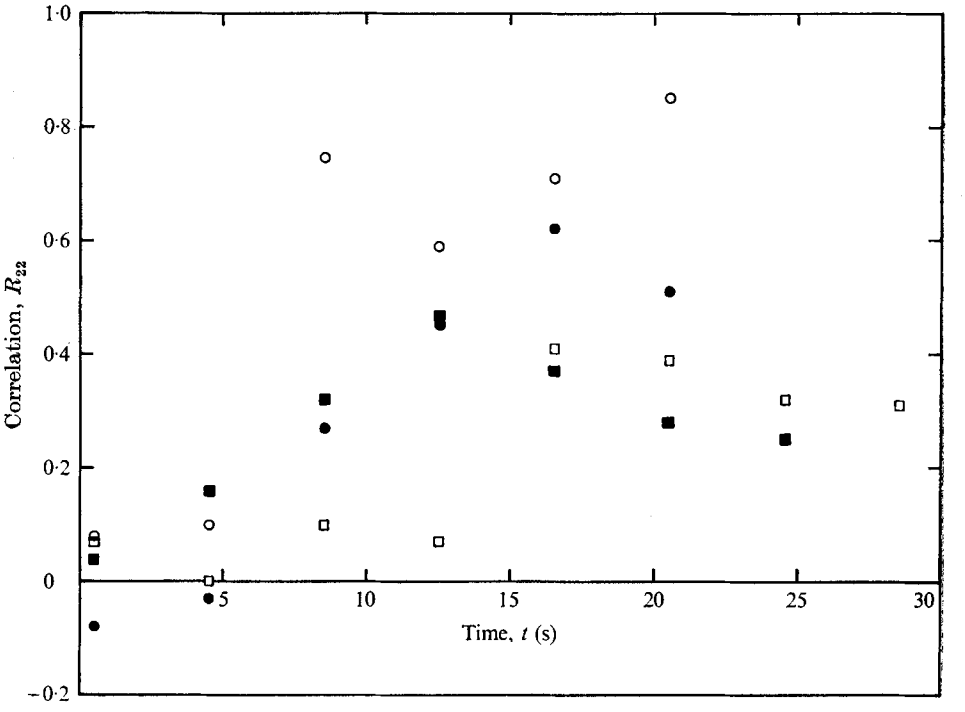

FIGURE 5. Two-point correlations R_{22} of azimuthal velocity components at different stages of the decay, for rotating ($\Omega = 2{\cdot}5$ rad s^{-1}) and non-rotating ($\Omega = 0$) experiments, with radial ($\Delta r = 34$ mm) and vertical ($\Delta z = 34$ mm) separations of the probes. ■, $\Omega = 0$, Δr; □, $\Omega = 0$, Δz; ●, $\Omega = 2{\cdot}5$, Δr; ○, $\Omega = 2{\cdot}5$, Δz.

either rough (experimental study by Hide & Collier, unpublished) or porous (theoretical study by Howard 1969), the spin-up time is reduced from its value $T_s = D/2\nu^{\frac{1}{2}}\Omega^{\frac{1}{2}}$ for smooth horizontal boundaries. Since the grids in their rest positions at the top and bottom of the annulus probably constitute rough *and* porous boundaries, an experimental determination of the spin-up time was made.

This was done by measuring the time required for a small change (about 10 %) in the rotation speed of the apparatus to communicate itself to the air inside. The azimuthal velocity of the air was measured using a single vertical hot-wire anemometer, held at rest with respect to the laboratory at a fixed radius in the annulus. The anemometer output voltage was low-pass filtered and monitored on the digital voltmeter. The exponential decay curves of relative air speed as a function of time indicated a spin-up time roughly proportional to $\Omega^{\frac{1}{2}}$, but smaller than the value given by the theory for smooth walls by a factor of about 2·1. We may therefore take the spin-up time in our apparatus (empirically) to be $T_s' = 0{\cdot}24D/\nu^{\frac{1}{2}}\Omega^{\frac{1}{2}}$, although the dependences on depth and kinematic viscosity have not been verified.

It should be noted for later reference that the spin-up times referred to here are e-folding times for the velocity. Kinetic-energy e-folding times are, of course, smaller by a factor of 2.

3.5. *Search for an effect of turbulence on the mean velocity*

As we shall be discussing in §5, the assumption implicitly made so far, that the mean velocity distribution (relative to the laboratory) remains a rigid-body rotation throughout the generation and decay of the turbulence, is open to question. An experiment was therefore carried out with the object of determining whether any mean flow was produced (relative to the rotating annulus) and, if so, with what vorticity distribution.

The hot-wire anemometer was used as in §3.4. The anemometer output voltage was low-pass filtered and recorded directly on a chart recorder. Turbulence was generated in the usual way with the apparatus rotating, and changes in the mean air speed past the probe were sought. The rotation rate was $1{\cdot}0\,\mathrm{rad\,s^{-1}}$ (chosen so that the initial energy of the turbulence was roughly equal to the energy difference between the rigid-body rotation and an irrotational motion with the same total angular momentum; see §5). Two sets of observations were made with the probe at radii of 384 mm and 524 mm respectively; i.e. approximately one-quarter and three-quarters of the way across the annulus. Any mean velocity change might have been expected to be of opposite sign at these two positions (see §5).

The results of these experiments (repeated several times) were entirely negative at both positions: no speed change was detected which could not be attributed to the small changes in velocity in the wake of the probe itself. In fact the smallest speed change which could have been detected (above the background 'noise') was estimated to be $\pm 10\,\mathrm{mm\,s^{-1}}$.

We therefore conclude that the mean flow produced in the annulus by the action of the turbulence is $0 \pm 10\,\mathrm{mm\,s^{-1}}$ at a rotation speed of $1{\cdot}0\,\mathrm{rad\,s^{-1}}$.

4. General discussion of the results

4.1. *Comparison of non-rotating case with wind-tunnel observations*

The measurements for $\Omega = 0$ may usefully be compared with wind-tunnel measurements of grid turbulence. We use the azimuthal intensity measurements for this purpose, partly because these extend to considerably higher values of t and partly for a reason indicated in §4.2.

Figure 6 shows the $\Omega = 0$ data from figure 3 replotted in the form $1/v'^2$ *vs.* t. The behaviour from $t = 8\,\mathrm{s}$ to $t = 60\,\mathrm{s}$ is well represented by

$$1/v'^2 = b(t - t_0)^m \tag{1}$$

with $b = 3{\cdot}5 \times 10^{-3}\,\mathrm{mm^{-2}\,s}$, $t_0 = 4{\cdot}5\,\mathrm{s}$ and $m = 1$. This corresponds to the initial-period decay law proposed by Batchelor (1953, p. 134) on the basis of experimental data obtained by Batchelor & Townsend (1948*a*) and Stewart & Townsend (1951). It has been suggested (Baines & Peterson 1951) that a somewhat higher value of the exponent m than 1 is more appropriate for wind-tunnel data, and recent work by Uberoi & Wallis (1967) seems to confirm this. We are not claiming that our results fit $m = 1$ better than other possibilities; small adjustments to the time origin allow a range of power laws to be fitted. However, figure 6

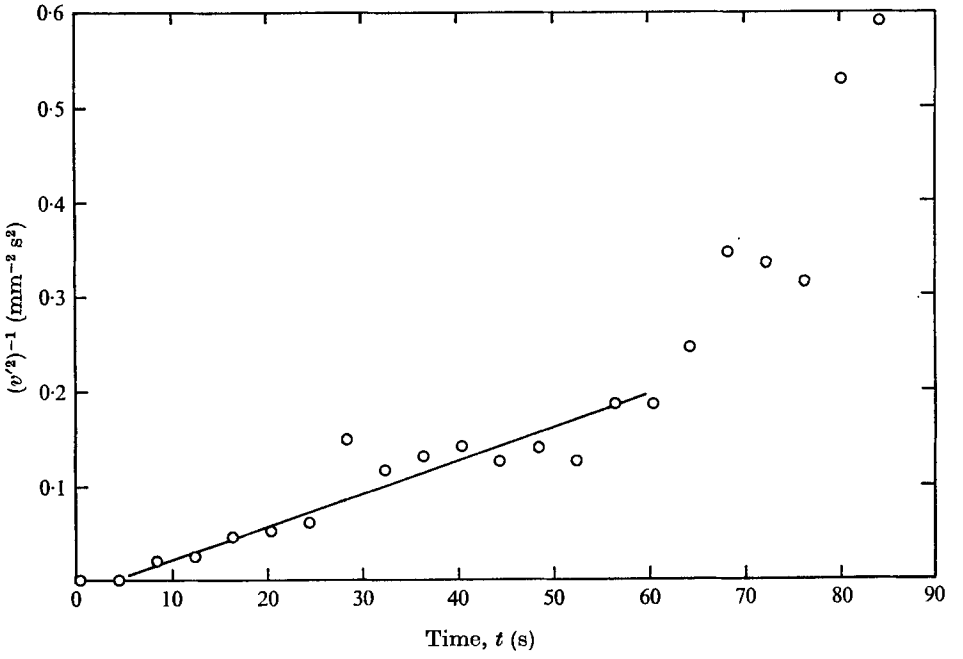

FIGURE 6. Initial-period decay law. Graph showing the reciprocal azimuthal turbulence intensity $(v'^2)^{-1}$ *vs.* t for the non-rotating experiment.

does demonstrate a significant similarity between the turbulence in our apparatus and that in a wind tunnel.

Moreover, (1) provides a convenient way of relating the time scale of our experiment to the distance downstream in a wind tunnel. Wind-tunnel results are conventionally expressed in the form

$$U^2/u'^2 = b'(x-x_0)/M, \tag{2}$$

where b' depends on the grid geometry. This corresponds to (1) when $m = 1$ and

$$U = b'/bM. \tag{3}$$

For a specified value of b', this enables an equivalent wind-tunnel velocity U to be determined. Batchelor (1953, p. 136) quotes a value of 134† for b' for the commonly used 5 : 1 square-mesh grid. Then with the above value of b and $M = 50$ mm, $U = 0{\cdot}77$ m s^{-1}. Thus the development at a particular time t in our experiment may be most directly compared with the development at a distance x behind a grid of this sort using the equation

$$(x-x_0)/M = \eta(t-t_0) \tag{4}$$

with $\eta = 15\,\mathrm{s}^{-1}$. It should be noted, however, that comparison with a different grid geometry requires the use of a different equivalent velocity U.

So far it has been assumed that the appropriate comparison with wind-tunnel experiments is with a grid of mesh length equal to the 50 mm hole spacing of our

† Although this may be untypically high (Sato 1951).

grids. Since the variation of b' with grid geometry reflects changes in the length scale of the turbulence relative to the mesh length, this needs further consideration. Baines & Peterson's (1951) results imply that the length scale at the start of the initial period increases markedly as d'/M (where d' is the bar diameter of the grid) increases. One might expect that, as the open-area ratio of the grid is decreased still further, the turbulence field is generated through the merging of an array of jets rather than of an array of wakes. This implies that the length scale will be governed by the size of the holes in the grid rather than the size of the solid parts, and so the above trend with d'/M should be reversed. This expectation is confirmed by considering the length scale l defined by

$$-du'^2/dt = u'^3/l. \tag{5}$$

Taking the start of the initial period in wind-tunnel grid turbulence to occur at $(x-x_0)/M = 10$, the value of l at this start is given by

$$l/M = (10/b')^{\frac{1}{2}}. \tag{6}$$

This initial l/M is thus 0·27 for the commonly used grid with $d'/M = 0{\cdot}2$ but rises to about 0·85 for $d'/M = 0{\cdot}5$ (on the basis of Baines & Peterson's results as analysed by Hinze 1959, p. 216). For our experiment, the initial period has started by $t = 6$ s† when l/M is equal to 0·42. Hence, as anticipated, comparison of our results with the wind-tunnel measurements using grids of fairly high open-area ratio is meaningful.

The period before (1) starts to apply is presumably to be regarded as a settling-down period during which the characteristics of the individual jets are lost, and a more homogeneous turbulence field arises. Using the equivalent wind-tunnel velocity estimated above, this period is markedly longer than the corresponding period in wind-tunnel turbulence; however, the generation processes are so different that one does not expect any close comparison.

In wind-tunnel experiments the initial period continues to $x/M \simeq 200$ and then departures from (1) occur in the direction of faster decay. In our experiments, (1) remains a good representation of the decay to times equivalent to considerably larger x/M. There are not, however, sufficient wind-tunnel measurements for $x/M > 200$ for one to know whether this is a significant difference in behaviour.

When departure from (1) does occur, at about $t = 60$ s, it is in the direction of faster decay (figure 6). By this time the Reynolds number $v'M/\nu$ has dropped to less than 10 (a consequence, of course, of the initial Reynolds number being much smaller than in most wind-tunnel experiments) and comparison with 'normal' turbulence may not be meaningful. The subsequent behaviour can be satisfactorily interpreted as a trend towards a final decay period as defined by Batchelor & Townsend (1948*b*) and Batchelor (1953). However, the experimental scatter becomes large here, and the data terminate when the Reynolds number is still about 4, so comparison with the various decay laws proposed for the final period (Ling & Huang 1970) is not possible.

† This is not apparent from figure 6 because of the spacing of the data points; it is based on a preliminary experiment in which the time intervals were shorter.

4.2. *Effect of rotation on decay rate*

The main effect of varying the rotation is apparent in figure 3: increasing the rotation rate results in more rapid decay of the turbulence. As mentioned in § 1, it was a particular purpose of these experiments to determine this trend. Its interpretation will form the basis of the discussion in subsequent sections of the dynamical process involved.

There is one exception to the above trend. The decay of w' for $\Omega = 0$ is more rapid than that for the lower non-zero rotation rates. This observation has been repeated in a second run. However, we are uncertain of the validity of this result, for three reasons. First, it proved more difficult to obtain negligible thermal stratification when the apparatus was not rotating than when it was. The $\Omega = 0$ observations were thus made with $N \simeq 0{\cdot}3\,\mathrm{rad\,s^{-1}}$. This seems likely to have its main effect on the vertical velocity fluctuations. Second, the measurements imply increasing anisotropy of the $\Omega = 0$ motion as time proceeds, not the behaviour expected from wind-tunnel measurements (Townsend 1956, §3.8). Third, the w' measurements at $\Omega = 0$ differ sharply from those that would be predicted by extrapolation of the measurements for non-zero Ω (whilst there is no such difference in the v' measurements). Hence, although it certainly remains a possibility to be investigated in further experiments that there is a trend reversal at low rotation rates, we do not incorporate this into our present interpretation of the results. We shall talk as if increasing Ω always results in faster decay. Two points may be made in this connexion. First, one expects, from symmetry considerations, that u' behaves like v' and so the total energy of the turbulence will still behave throughout in the way shown by v' – qualitatively if not quantitatively. Second, remarks made (for simplicity) in terms of the contrast between non-rotating and rotating behaviour of v' do apply to w' if, instead, low and high rotation rates are compared.

Figure 7 displays the effect of rotation rate on decay rate in a different way. In figure 7 (*a*), the values of t at which v' has fallen to each of several fractions of its initial value are shown as functions of Ω. Figure 7 (*b*) shows the equivalent plots for w'. The line on each graph has a slope of $-\frac{1}{2}$. The probable significance of the fact that this provides a good representation of the trend of the data for the later stages of decay will be considered in §6.1.

The faster decay with more rapid rotation can, as noted in § 1, be considered as an example of the stabilizing influence of rotation. However, this general remark does not indicate what happens to the energy removed from the turbulence, a matter of evident importance in understanding the dynamical processes. There are, in principle, three possibilities: that the structure of the turbulence is changed in a way such as to increase the local viscous dissipation; that the energy is transferred to the mean motion of the fluid; or that the energy is transported to the edges of the fluid region, where viscous dissipation occurs in boundary layers. We believe that the first possibility can be immediately rejected; it is difficult to see how rotation could cause such a change, and the experimental data (see, in particular, the spectra; §§3.2 and 4.3) contain no evidence of a change of the required type. We also think that the second possibility may be eliminated,

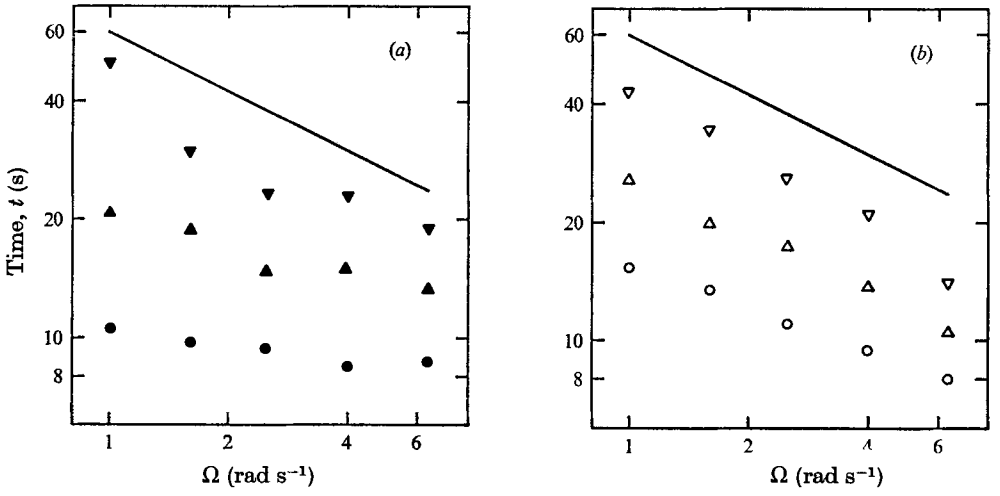

FIGURE 7. The times t as functions of Ω at which (*a*) the azimuthal component v' and (*b*) the vertical component w' of r.m.s. turbulence intensity have decayed to various fractions f of their values at $t = 0{\cdot}5$ s. ●, ○, $f = 0{\cdot}05$; ▲, △, $f = 0{\cdot}025$; ▼, ▽, $f = 0{\cdot}0125$.

but this requires much more detailed consideration, which will be postponed until §5. A model that can account for the observations, based on the third possibility, will be developed in §6.

Ω (rad s^{-1})	0	1·0	1·6	2·5	4·0	6·4
Average v'/w'	1·65	1·32	1·24	1·24	1·54	1·73

TABLE 2

Comparison of the v' and w' decay curves shows that the initial anisotropy of intensities (table 1) persists but does not usually increase. Table 2 lists the values of v'/w', averaged in each case over the time for which both quantities were measurable. No systematic variation with Ω or difference from the initial values given in table 1 is apparent. Also, for the most part, the individual values for a given rotation rate (not displayed) do not show any systematic variation with time. (Exceptions are the extreme cases $\Omega = 0$, discussed above, and $\Omega = 6{\cdot}4$ rad s^{-1}, for both of which v'/w' increases to above 2 as time proceeds.) The implication seems to be that the decays of the two components remain quite tightly coupled. This was not necessarily to be expected, since a Taylor–Proudman effect causing anisotropy in the length scales could well destroy the usual coupling through the continuity equation.

4.3. *Spectra*

The scatter in figures 4 (*a*)–(*e*) makes it difficult to discern trends immediately. However, close inspection reveals certain features on which comment may be made. In this section we note some general features of the spectral data; in §6.2, the results will be re-analysed in connexion with a particular model of the decay.

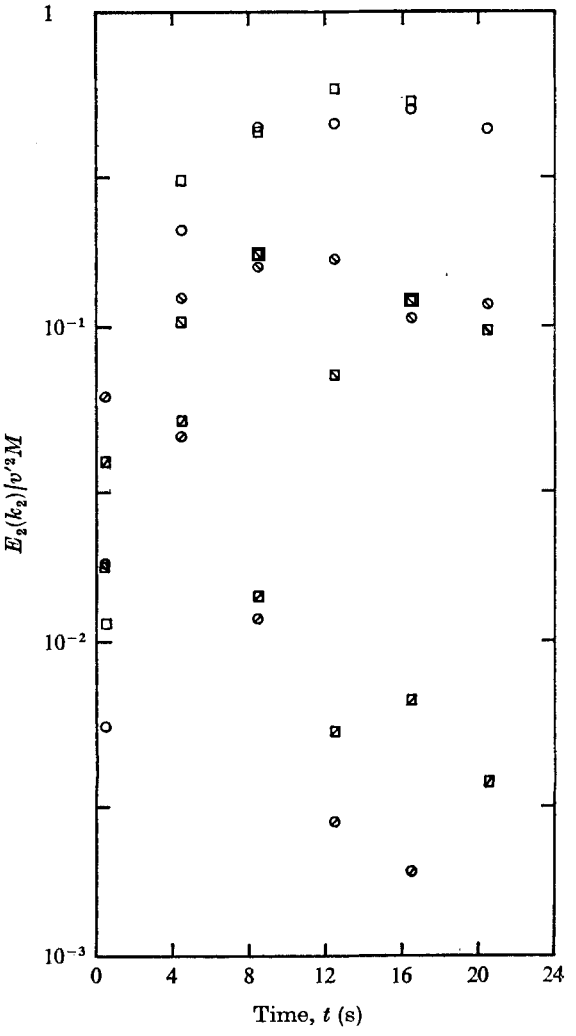

FIGURE 8. The development with time t of different wavenumber components of the normalized energy spectra of the azimuthal velocity component in rotating ($\Omega = 2{\cdot}5\,\mathrm{rad\,s^{-1}}$) and non-rotating ($\Omega = 0$) experiments. □, $\Omega = 0$, $k_2M = 1{\cdot}35$; ○, $\Omega = 2{\cdot}5$, $k_2M = 1{\cdot}35$; ⧅, $\Omega = 0$, $k_2M = 2{\cdot}9$; ⊘, $\Omega = 2{\cdot}5$, $k_2M = 2{\cdot}9$; ⧄, $\Omega = 0$, $k_2M = 7{\cdot}4$; ⊘, $\Omega = 2{\cdot}5$, $k_2M = 7{\cdot}4$.

Figure 4 (*a*) shows spectra during the traverse of the grids. One expects these to be strongly influenced by the details of the turbulence generation process. The marked peaking of all the spectra in the vicinity of $k_2M = 8$ (which corresponds to a wavelength $2\pi/k_2$ of about 40 mm) presumably reflects the jet structure of this process. (It is a bit surprising, therefore, that for $\Omega = 0$ the peaking is more marked in the horizontal-motion spectrum than in the vertical-motion spectrum.) For both E_2 and E_3, the peak is noticeably sharper in the rotating case compared with the non-rotating case. This suggests that rotation does have some effect on the jets, despite their high Rossby number.

In the subsequent development of the turbulence, one may expect the spectra

for $\Omega = 0$ to take on the form characteristic of grid turbulence. Figure 4(*d*) includes an E_u spectrum (the counterpart of our E_2) measured by Uberoi & Wallis (1969) behind a wooden grid with $d'/M = 0{\cdot}25$ in a wind tunnel; this applies to the corresponding stage of development on the basis of the equivalent wind-tunnel velocity evaluated as in §4.1 (approximating the decay curve in Uberoi & Wallis (1967) by an expression of the form of (2)). The fact that our spectrum falls off much more rapidly at large $k_2 M$ is accounted for by the much lower Reynolds number of our turbulence.

In most of the spectra the lowest $k_2 M$ point shows an unexpected drop in E_2 or E_3 below its maximum value. However, this wavenumber corresponds to a wavelength $2\pi/k_2$ of 500 mm, compared with the annulus width of 300 mm. The motion of this length scale is thus likely to be modified by the presence of the boundaries (cf. Comte-Bellot & Corrsin 1971, appendix E).

For the non-rotating case, one may also compare the relationship between the $E_2(k_2)$ and $E_3(k_2)$ spectra with that corresponding to isotropic turbulence. The scatter is too large to allow quantitative comparison, but qualitatively the relationship is of the form expected, with $E_3/w'^2M < E_2/v'^2M$ at low k_2 but not falling so rapidly as k_2 increases. This is immediately apparent in the spectra for $t = 4{\cdot}5$ s and can be seen in subsequent ones; e.g. E_3/w'^2M is less than E_2/v'^2M at $k_2 M = 1{\cdot}35$ but greater at $k_2 M = 2{\cdot}9$ for all times (except $t = 0{\cdot}5$ s).

Turning to the effect of rotation on the spectra, one notes a strong similarity between the E_2/v'^2M curves for $\Omega = 0$ and $\Omega = 2{\cdot}5\,\mathrm{rad\,s^{-1}}$. This is particularly remarkable for $t = 8{\cdot}5$ s, when the two sets of points are almost coincident (although the intensities have become significantly different by this time), but the differences at other times are mostly small and not apparently systematic. This is not due to a general similarity of all the spectra; in both cases, the spectral distributions are changing with time, as is illustrated by figure 8, which shows how E_2/v'^2M varies with time for selected values of k_2. The different trends for different wavenumbers but similar trends for different rotation rates are apparent. In §6.2 we shall be developing a model which implies that the factors determining spectral distributions are quite different in the rotating and non-rotating cases. It therefore seems that the similarity noted here must be a rather remarkable coincidence. However, we have noted it in case it has some underlying significance that we have not perceived.

The E_3/w'^2M curves also show similarities in their development for the rotating and non-rotating cases. However, now a systematic difference is to be seen at the low wavenumber end of the spectrum. At $k_2 M = 0{\cdot}63$, E_3/w'^2M is larger for $\Omega = 2{\cdot}5\,\mathrm{rad\,s^{-1}}$ than for $\Omega = 0$ in a systematic way from $t = 8{\cdot}5$ s onwards. (The same is true at $k_2 M = 1{\cdot}35$, although here the differences are so small that their significance is questionable.) Although extrapolation of the results to $k_2 = 0$ to determine an integral length scale (Hinze 1959, p. 172) is hindered by the effect noted above of the finite apparatus size, this presumably indicates that the integral scale is increased by the rotation as the turbulence decays. This inference ties up with the implications of the correlation measurements to be discussed in §4.4 (although we do not know why it should be apparent in the $E_3(k_2)$ data and not in the $E_2(k_2)$ data).

4.4. *Correlations*

The salient features of the correlation measurements are contained in the numbers quoted at the end of §3.3. We now comment on the significance of these results.

The near equality of $R_{22}(\Delta r)$ and $R_{22}(\Delta z)$ for $\Omega = 0$ suggests that the non-rotating turbulence is isotropic in length scale even though apparently not in intensity (§4.1).

The most striking effect of rotation is the large increase in $R_{22}(\Delta z)$. This is the principal result of the correlation measurements since these provide the only way of looking for anisotropy in length scale. It is clear that such anisotropy exists in just the way that one would expect if the Taylor–Proudman theorem could be applied to the motion.

The measurements also indicate an increase in the length scale perpendicular to the rotation axis compared with the non-rotating case; i.e. $R_{22}(\Delta r)$ also increases although not to the same extent as $R_{22}(\Delta z)$. This is a similar inference to that made from the behaviour of $E_3(k_2)$ (but not of $E_2(k_2)$†) at low k_2. This observation may also be related to the Taylor–Proudman theorem, although not so directly, if the theorem is interpreted as imposing a 'two-dimensional' structure on the turbulence. It is known (Fjørtoft 1953; Kraichnan 1967; Batchelor 1969) that any energy transfer between wavenumbers in two-dimensional turbulence must occur simultaneously towards higher wavenumbers and towards lower wavenumbers. Hence an increase in length scale may be expected as compared with three-dimensional turbulence in which the transfer is dominantly towards higher wavenumbers.

Thus, in general, the length-scale relationships revealed by the correlation measurements may be interpreted by a simple application of ideas associated with the Taylor–Proudman theorem. Incorporation of these ideas into the overall picture of the motion inferred from all types of measurement is not so simple. Indeed, we have already seen (§4.2) that the decoupling of the axial and azimuthal velocity fluctuations that one would expect to be associated with the above processes does not occur. We shall return to this matter in §7.

The experimental results in §§3.4 and 3.5 will not be discussed here, but will be drawn on in subsequent sections.

5. The vorticity expulsion hypothesis

The possibility mentioned in §4.2 that the turbulence loses energy by transfer to the mean motion would imply that the presence of the turbulence causes a departure of the mean velocity distribution from a rigid-body rotation. It has several times been suggested that such an interaction might occur. Although the idea has taken various forms (e.g. Starr 1968; Scorer 1965), these are all

† It should be noted that, in principle, with the anisotropy imposed by the rotation, the length scales to be inferred from $R_{22}(\Delta r)$, $E_2(k_2)$ and $E_3(k_2)$ are all different. There is no requirement that any two should behave in the same way, although, on any particular interpretation, one probably expects all three to do so.

somewhat related, and it is convenient to discuss the hypothesis in terms of the vorticity expulsion concept enunciated by Gough & Lynden-Bell (1968). The arguments in favour of the hypothesis are not at all rigorous and the experimental evidence is inconclusive (Bretherton & Turner 1968; Strittmatter, Illingworth & Freeman 1970). However, it is clearly a possible explanation of the more rapid decay of the turbulence when there is rotation.

For our experiment the hypothesis would imply that the turbulence interacts with the basic rotation to change the mean velocity distribution (measured with respect to stationary co-ordinates (r, ϕ, z)) from

$$V = \Omega r \tag{7}$$

towards (except in thin boundary layers on the walls)

$$V = K/r, \tag{8}$$

K being determined by the requirement that the total angular momentum should be unchanged. This involves an increase in the kinetic energy of the mean motion, which must be provided by a decrease in the kinetic energy of the turbulence. If the turbulence does not contain enough energy for this process to occur completely, then the hypothesis implies that the mean velocity would be changed to one with vorticity between zero and 2Ω. We suppose that this may be represented by a combination of rigid-body rotation and irrotational motion in the form

$$V = \Omega' r + K/r, \quad \text{where} \quad \Omega' < \Omega. \tag{9}$$

For a cylindrical annulus of inner and outer radii a and $2a$, conservation of angular momentum gives

$$V = \Omega' r + 5(\Omega - \Omega')a^2/2r. \tag{10}$$

Applying this equation, the observation (§3.5) that V changed by less than $10\,\mathrm{mm\,s^{-1}}$ at both $r = 384\,\mathrm{mm}$ and $r = 524\,\mathrm{mm}$ implies that $\Omega - \Omega'$ remained less than $0{\cdot}025\,\mathrm{rad\,s^{-1}}$ (at $\Omega = 1\,\mathrm{rad\,s^{-1}}$). Two questions are raised by this negative result: does it provide significant evidence against the hypothesis; and does it rule out the process as an explanation of the more rapid decay of the turbulence observed in the rotating system?

We shall not discuss the former here. Decaying-turbulence experiments are not suitable for testing the hypothesis, since the expulsion time scale is always large compared with the eddy-turnover time scale and thus with the decay time scale. Complete expulsion is thus unlikely. Quantitative consideration of how much mean velocity redistribution might be expected in a given case is a complicated matter and would take us too far from the theme of the present paper.

There remains the possibility, however, that an undetectable mean velocity redistribution involves an energy transfer that amounts to a significant fraction of the turbulence energy. The second question therefore requires consideration, and, in fact, we look at it first through direct energy considerations and second in a less direct way.

The increase in kinetic energy per unit mass associated with the velocity distribution (10) above its initial value corresponding to $\Omega' = \Omega$ is

$$\tfrac{5}{12}(5\ln 2 - 3)a^2(\Omega - \Omega')^2 = 0{\cdot}19a^2(\Omega - \Omega')^2. \tag{11}$$

In the time interval ($5 < t < 10$ s) in which the differences in decay rate have become apparent, but in which the energies involved are still significant, there is a difference in v'^2 between the cases $\Omega = 0$ and $\Omega = 1\,\mathrm{rad\,s^{-1}}$ of about $20\,\mathrm{mm^2 s^{-2}}$. Taking this to imply a difference in $\frac{1}{2}q'^2$ of about $20\,\mathrm{mm^2 s^{-2}}$, the transfer of this energy difference to the mean motion would imply a value of $\Omega - \Omega'$ of about $0{\cdot}035\,\mathrm{rad\,s^{-1}}$. This is just greater than the minimum observable value, but allowing for the imprecision of the measurements, one can scarcely rule out the process on these grounds.

However, another method of analysing the data is more productive. This uses the fact that the transfer of energy from the turbulence to the mean flow involves the generation of a Reynolds stress, the size of which is limited by the turbulence intensity. Supposing that the transfer of energy to the mean motion is the only process changing the turbulence energy,

$$\frac{1}{2}\frac{\partial q'^2}{\partial t} = -\overline{uv}r\frac{\partial}{\partial r}\left(\frac{V}{r}\right) \tag{12}$$

(cf. Townsend 1956, equation 12.1.7). Substituting (10) gives

$$-\frac{1}{q'^2}\frac{\partial q'^2}{\partial t} = 10\zeta(\Omega - \Omega')a^2/r^2, \tag{13}$$

where $\zeta = -\overline{uv}/q'^2$. In the absence of any process producing strong anisotropy of the turbulence in planes perpendicular to the rotation axis, ζ must remain small. Even in the presence of such a process, ζ cannot exceed $\frac{1}{2}$ (or $\frac{1}{3}$ if $w' = v'$) and is unlikely to approach very close to this maximum. Using the observation that $\Omega - \Omega' < 0{\cdot}025\,\mathrm{rad\,s^{-1}}$, this indicates that at $r/a = 1{\cdot}5$

$$-\frac{1}{q'^2}\frac{\partial q'^2}{\partial t} < 0{\cdot}05\,\mathrm{s^{-1}}. \tag{14}$$

This may be compared with $-v'^{-2}\partial v'^2/\partial t$ (obtained from the measurements of v'^2 at $\Omega = 1\,\mathrm{rad\,s^{-1}}$), which is typically around $0{\cdot}105\,\mathrm{s^{-1}}$ at the relevant stage of decay. Comparison with the case $\Omega = 0$ indicates that no more than about a third of this decay rate can be produced by the normal viscous dissipation process. The remainder is distinctly larger than the maximum possible according to relationship (14). Even if experimental inaccuracies might be invoked to bring this remainder within the range of relationship (14), the maximum represents such an extreme case that one does not expect it to be approached. It thus seems certain that this mechanism cannot account for the observed decay rate.

Clearly measurements of the Reynolds stress would be desirable, and we hope to carry them out along with measurements of u'. However, we do not believe that these measurements could affect the above conclusion.

6. An inertial-wave model of the decay

6.1. *General features*

The third possibility mentioned in §4.2, that the energy is transported to the walls and dissipated there in boundary layers, arises in a rotating fluid through the action of inertial waves (Phillips 1963; Greenspan 1968, §4.2). These are

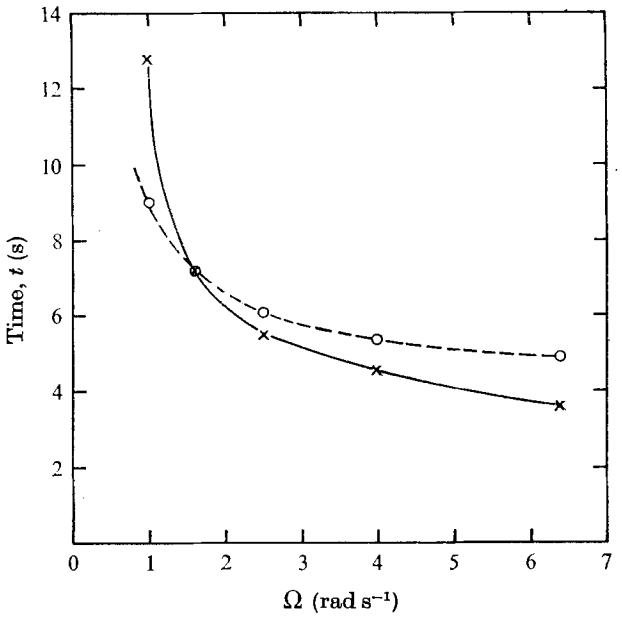

FIGURE 9. The times t after generation of the turbulence at which (i) the Rossby number $v'/M\Omega$ is equal to 0·1 (× , solid line) and (ii) the parameter $J = v'L/(\Omega\nu)^{\frac{1}{2}}M$ is equal to 10 (○, dashed line) for different rotation speeds.

generated by any oscillation of angular frequency less than 2Ω, and will thus play a role in the dynamics of the turbulence when a significant part of its frequency spectrum is in this range. We may take the frequency associated with an eddy of size $2\pi/k$ as

$$\omega \sim vk. \tag{15}$$

Thus, those wavenumbers for which the Rossby number $vk/2\Omega$ is less than about 1 will tend to involve inertial-wave generation. The criterion for this wave generation to change the character of the turbulence strongly from that of turbulence in a non-rotating fluid may be written as

$$v/M\Omega \ll 1. \tag{16}$$

For a given Ω, this criterion becomes more strongly fulfilled as the turbulence decays. One may expect the turbulence to be initially little different from that in a non-rotating fluid, but to be increasingly modified by the action of inertial waves as time proceeds. Figure 9 shows the value of t at which $v'/M\Omega = 0{\cdot}1$ (using the experimentally observed values of v') as a function of Ω.† It is clear that we are dealing primarily with low Rossby number turbulence. For this to lead to a significant change in the decay rate, it is necessary also that the occurrence of inertial waves should introduce a new dissipation process, a matter discussed below.

It should be noted that relationship (16) is essentially a negative criterion,

† The significance of the other curve on this figure is explained below.

a criterion for the turbulence not to remain unaffected by the rotation, rather than a criterion for the occurrence of any particular new process. The relationship $\omega = 2\boldsymbol{\Omega} \cdot \mathbf{k}/|\mathbf{k}|$ between frequency and wavenumber for an inertial wave is quite different from that for the turbulence. For this reason, one cannot say much about the detailed pattern of inertial waves that might be generated. It is an attractive notion to use some accepted representation of a turbulence field as an initial condition for a calculation of the evolution of inertial waves. However, one does not know whether to specify a frequency spectrum or a wavenumber spectrum, and one cannot specify both ! Evidently, the transitional period, when the Rossby number is about 1 and the turbulence is being affected by the rotation but not completely changed in character, has a strong effect on the details of the subsequent behaviour. Nevertheless it is reasonable to suppose that the ultimate behaviour at low Rossby number resembles a random superposition of (weakly interacting) inertial waves, and to use the properties of such waves in an interpretation of the observed behaviour.

The relevant properties are described by Phillips (1963) and Greenspan (1968). The waves travel with a group velocity $|\mathbf{v}_g|$ of order of magnitude $2\Omega/k$. On reflexion at a boundary, there is a fractional loss of energy ϵ of order of magnitude $(\nu k^2/\Omega)^{\frac{1}{2}}$. If ϵ is small, a wave decays by a process of multiple reflexions with an e-folding time τ given by

$$\tau \sim L/\epsilon v_g \sim (L^2/\nu\Omega)^{\frac{1}{2}}, \tag{17}$$

where L is the distance travelled between reflexions, i.e. the size of the enclosure. τ is thus independent of the magnitude of the wavenumber (although its precise value does depend on the direction of the wavenumber, as we shall be discussing in §6.3). It is essentially the spin-up time for the apparatus.

The observed decay rates strongly suggest that the above process may be the principal mechanism for the later stages of decay when the system is rotating. Figure 7 has shown that there is approximate proportionality of decay times to $\Omega^{-\frac{1}{2}}$; the arbitrariness in the choice of time origin does not much affect the form of these graphs at large times. Moreover, at each Ω, the decay time is very similar in size to the spin-up time.

This process, acting alone, would give an exponential variation of energy with time. The individual decay curves do not exhibit markedly exponential forms, although the departures from such a form are not sufficiently systematic to be summarized simply.† Another feature of the observations not predicted by the above process is the evolution of the spectra with time. Both these apparent discrepancies may be accounted for by the fact that the waves are also subject to internal viscous dissipation. This proceeds at a rate $2\nu k^2 E$, just as in a non-rotating fluid, and is important only at the high wavenumber end of the spectrum. We thus postpone more quantitative comparison of the model with the observations to §6.3: after the spectral data have been analysed in this context in §6.2.

† The data are probably somewhat better represented by

$$v'^2 \propto w'^2 \propto [(t-t_0)\,\Omega^{\frac{1}{2}}]^{-n}$$

than by an exponential, with n between 2 and 3·5 (the wide range reflects the fact that, as with wind-tunnel turbulence, different values of n can be fitted by different choices of the time origin t_0).

It is useful, however, at this stage to obtain one numerical coefficient from the total intensity data. The above comments notwithstanding, it is possible to fit the data to

$$v'^2 \propto w'^2 \propto \exp(-\alpha\Omega^{\frac{1}{2}}t) \tag{18}$$

as a general approximate representation. Making such a fit, weighted towards the later stages of decay and the more rapid rotation rates, gives $\alpha = 0{\cdot}105 \pm 0{\cdot}02\,\mathrm{s}^{-\frac{1}{2}}$. Putting

$$\alpha = B\nu^{\frac{1}{2}}/L \tag{19}$$

in accordance with the model (and taking L as the width or depth of the annulus, 0·30 m) gives the numerical constant B as 8.

The above interpretation implies that the overall size L of the system enters as an important parameter. Application of the results to geophysical situations will, in general, be inhibited by this. An important non-dimensional parameter in this respect is the ratio of the time scale τ to the time scale l/v for the normal decay process in a non-rotating fluid. This ratio is

$$J = \frac{L}{(\Omega\nu)^{\frac{1}{2}}}\frac{v}{l} = (Ro\,Re)^{\frac{1}{2}}L/l. \tag{20}$$

If

$$J \gg 1 \tag{21}$$

the reflecting-wave process produces much slower decay than the normal process and one would not expect to observe results like ours. Relationship (21) is likely to be fulfilled in many practical situations. It is not, of course, fulfilled in our rotating experiments, except possibly during the early stages of decay. Figure 9 includes a curve showing, as a function of Ω, the time at which J falls below 10 (taking $l = M$ and $v = v'$). The fact that this is a little above the other curve for the higher values of Ω suggests that a few of the observations correspond to conditions in which the effect of rotation was strong (low Rossby number) but in which the decay process discussed above was relatively weak. Any strong additional effect of the rotation, such as the inhibition of decay by the turbulence becoming two-dimensional as mentioned at the end of §1, might have had an opportunity to show up here. In this region, departures from the non-rotating behaviour are actually slight.

In principle, the most important further stage in investigating turbulence in rotating systems is probably experimentation in conditions in which (21) is fulfilled throughout. In practice, such conditions may be very difficult to achieve.

6.2. *Decay of spectral components*

The model proposed in §6.1 for the decay of turbulence in a rotating fluid implies that the transfer of energy between wavenumbers is a less dominant feature than in conventional turbulence. It may thus be of interest to examine the decay of individual spectral components. This can be done for only a limited number of components, because in other cases problems with the signal-to-noise ratio prevented the data from extending to large enough values of t. However, it will be seen that the few cases that can be so analysed do provide further evidence relevant to the model.

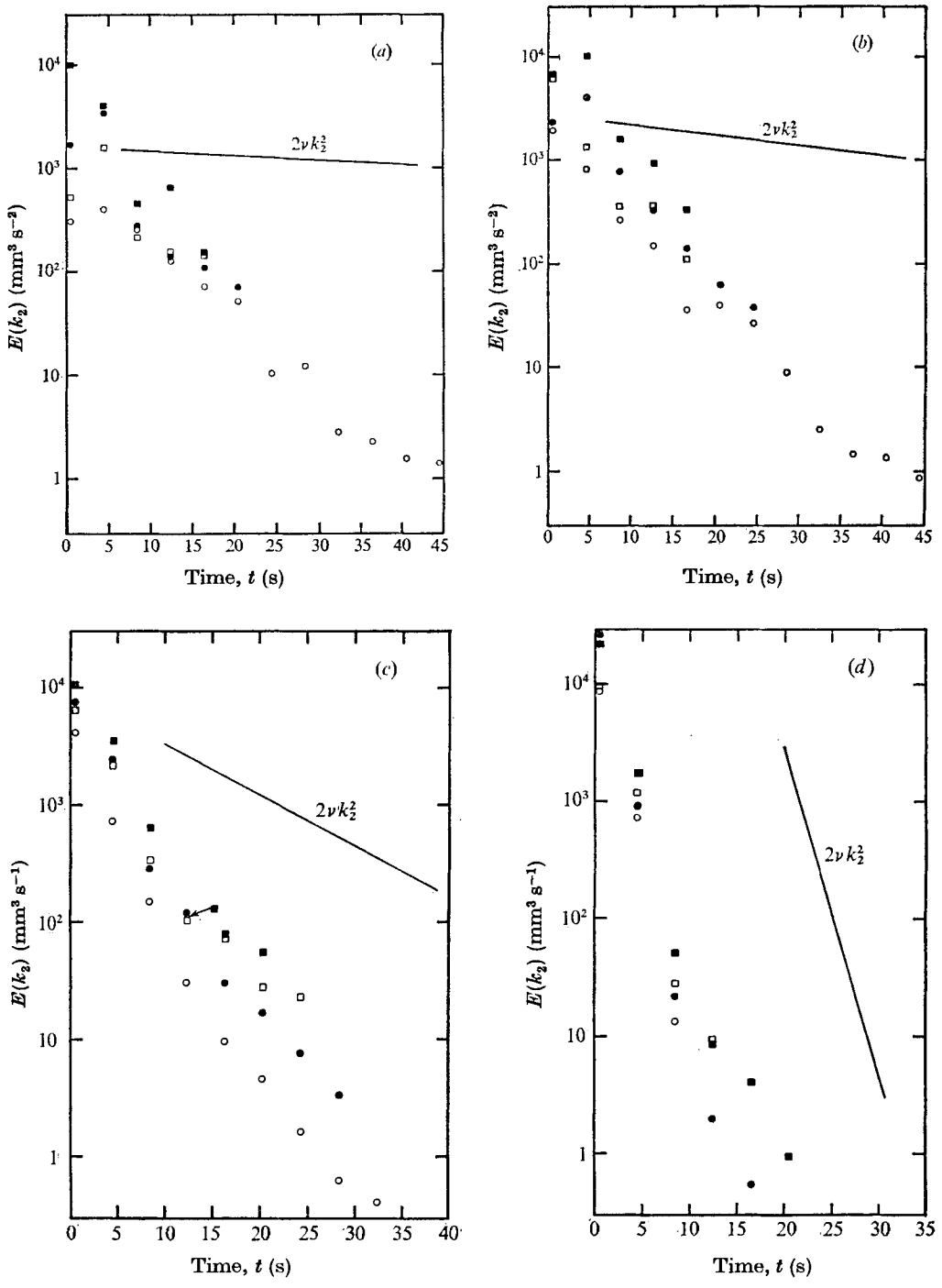

FIGURE 10. The decay of individual spectral components with time t, plotted on a log–linear scale, for various wavenumbers: (*a*) $k_2M = 0{\cdot}63$; (*b*) $k_2M = 1{\cdot}35$; (*c*) $k_2M = 2{\cdot}9$; (*d*) $k_2M = 7{\cdot}4$. Data from rotating ($\Omega = 2{\cdot}5$ rad s^{-1}, circles) and non-rotating ($\Omega = 0$, squares) experiments and for azimuthal (closed points) and vertical (open points) velocity components are plotted on each graph. The straight line on each graph has slope corresponding to a decay constant of $2\nu k_2^2$.

For comparison, the results for $\Omega = 0$ are treated in the same way. Further, since this is a somewhat novel presentation of turbulence data, it is helpful to know how wind-tunnel data look when so treated; Sato's (1952) data for a grid with $d'/M = 0{\cdot}2$ are thus also presented in this form.

Figures 10 (*a*)–(*d*) show log–linear plots of $E_2(k_2, t)$ and $E_3(k_2, t)$. The lines on the graphs correspond to $E^{-1}\,\partial E/\partial t = -2\nu k_2^2$. They thus give an indication of the direct viscous action at each wavenumber. The fact that one can measure only one-dimensional spectra limits this indication. But the order of magnitude of the direct viscous action in relation to the actual decay rate is informative. The actual direct viscous action will always be stronger than that indicated, since $E(k_2)$ receives contributions from all k greater than k_2; for higher wavenumbers, where E is decreasing rapidly with k_2, it will not be very much stronger (see, for example, Hinze 1959, equations 3-72, 3-73).

The wind-tunnel results in figure 11 demonstrate the well-known properties of this type of turbulence. At any time, the higher wavenumbers are decaying more rapidly than the lower, but the differences are much less than those between the direct viscous decay rates. The relationship between actual and viscous decay rates demonstrates the loss of energy at low wavenumbers and gain at high wavenumbers by spectral transfer. At every wavenumber, $-E^{-1}\,\partial E/\partial t$ decreases as time proceeds; as the Reynolds number decreases, some wavenumbers change from being losers of energy by spectral transfer to receivers.

Our results for $\Omega = 0$ are generally consistent with this – allowing for the fact that the initial Reynolds number is much smaller. The quality and extent of the data are not good enough to show the decrease in $-E^{-1}\,\partial E/\partial t$ with time very clearly. However, it must occur: an extension of the graphs to higher t without such a decrease would produce results that were quite inconsistent with the measured total v'^2 and w'^2.

The results for $\Omega = 2{\cdot}5\,\mathrm{rad\,s^{-1}}$, on the other hand, can be represented much more closely as exponential decays. For a few cases, the data extend to quite large t and straight-line regions are apparent for both E_2 and E_3 in figures 10 (*a*)–(*c*). These are all for the lower wavenumbers, and the decay rates are faster than the direct viscous decay rates, as would be expected if an additional linear mechanism, such as that proposed in § 6.1, has been introduced by the rotation. At higher wavenumbers, the data are much less satisfactory, but in the one case where one can say anything, the decay appears to be somewhat *slower* than the minimum viscous decay rate (see also table 3 below); possibly spectral transfer to higher wavenumbers still plays some part in the dynamics.

Generally, however, it seems appropriate to interpret the results by supposing that the decay of a component of wavenumber $\mathbf{k}$ is governed by an equation of the form

$$\partial E/\partial t = -[C(\Omega\nu)^{\frac{1}{2}}/L + 2\nu k^2]E. \tag{22}$$

The coefficient C should be independent of the magnitude of $\mathbf{k}$. But it is to be expected to depend on the direction of $\mathbf{k}$ in a complex way related to the geometrical details of the particular apparatus. The development of a one-dimensional spectrum thus becomes even more problematical than usual. It nevertheless seems worthwhile to try to use the spectral data to test the model

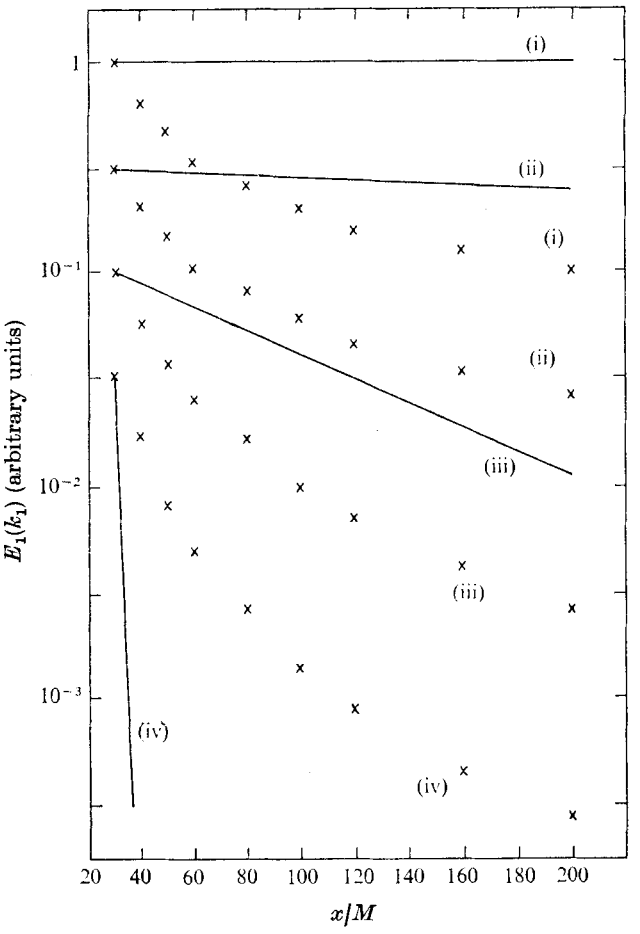

FIGURE 11. The wind-tunnel data of Sato (1952) plotted, on a log–linear scale, to show the decay of individual spectral components of longitudinal velocity with distance x downstream from the grid for various wavenumbers: (i) $k_1M = 0{\cdot}38$; (ii) $k_1M = 2{\cdot}9$; (iii) $k_1M = 11{\cdot}3$; (iv) $k_1M = 75{\cdot}5$. The lines have slopes corresponding to decay constants of $2\nu k_1^2$. The ordinate scale is arbitrary and the relative positions of data for different k_1 are without significance (being equally spaced at $x/M = 30$). (Note: k_1 is 2π times the quantity Sato denotes as 'wavenumber'.)

and in particular to obtain an estimate for C. In the absence of any better procedure, we have simply ignored the fact that the measured spectra are one-dimensional and not three-dimensional; i.e. the data of figures 10 (*a*)–(*d*) have been examined for a fit to

$$\partial E/\partial t = -\beta E = -(\gamma + 2\nu k_2^2)E. \tag{23}$$

Table 3 shows decay rates β for the $\Omega = 2{\cdot}5\,\mathrm{rad\,s^{-1}}$ data, obtained by least-squares fitting to points from $t = 8{\cdot}5\,\mathrm{s}$ onwards in figures 10 (*a*)–(*d*). From these, values of γ are calculated as shown in the table. Apart from the case of highest k_2 (on which comment has been made above), the variations in γ are small and not systematic. Taking an average value of γ as $0{\cdot}14\,\mathrm{s^{-1}}$ gives C in (22) as 6·8.

	k_2 (mm^{-1})	β (s^{-1})	$2\nu k_2^2$ (s^{-1})	$\gamma = \beta - 2\nu k_2^2$ (s^{-1})
E_2	0·0126	0·112 ± 0·011	0·005	0·11 ± 0·01
	0·027	0·194 ± 0·011	0·022	0·17 ± 0·01
	0·058	0·222 ± 0·012	0·10	0·12 ± 0·01
	0·147	0·46 ± 0·08	0·65	−0·2 ± 0·1
E_3	0·0126	0·157 ± 0·011	0·005	0·15 ± 0·01
	0·027	0·167 ± 0·011	0·022	0·145 ± 0·01
	0·058	0·242 ± 0·016	0·10	0·14 ± 0·02

TABLE 3

6.3. *Numerical comparison*

We now have two values for the numerical coefficient involved in a decay by the process envisaged: the quantity B (= 8) in § 6.1 and the quantity C (= 6·8) in § 6.2. The agreement between them is very satisfactory, particularly since B should in principle be rather larger than C, because the direct viscous decay has not been extracted in the evaluation of the former. Also for this reason, C may be regarded as the more precise coefficient. On the other hand, it should be remembered that the spectral measurements from which C is derived were made only for $\Omega = 2{\cdot}5$ rad s^{-1}, whereas B is based on data for several different values of Ω.

For comparison with these results, Phillips' theory needs to be considered in more detail than in the order-of-magnitude form used in § 6.1.

The loss of energy on reflexion depends in a complex way on the relative orientations of the axis of rotation, the wavenumber vector and the normal to the reflecting surface. Any full theory would thus be both complicated and applicable only to the particular geometry of our apparatus. We consider instead three geometrically simple situations, which provide relevant examples of the values of the coefficient.

An important parameter of inertial waves is θ, the angle between the wavenumber $\mathbf{k}$ and the axis of rotation. The angular frequency of the wave

$$\omega = 2\Omega \cos\theta. \tag{24}$$

The group velocity has magnitude

$$|\mathbf{v}_g| = 2\Omega \sin(\theta)/k \tag{25}$$

and is directed at right angles to $\mathbf{k}$ in the plane of $\mathbf{k}$ and $\boldsymbol{\Omega}$, i.e. at an angle θ to the horizontal (the rotation axis being vertical).

Each of the three examples consists of two infinite parallel surfaces a distance L apart. In case (i), these planes are horizontal. In case (ii), they are vertical and the plane containing $\boldsymbol{\Omega}$, $\mathbf{k}$ and $\mathbf{v}_g$ intersects them at right angles. In case (iii), they are again vertical but the plane containing $\boldsymbol{\Omega}$, $\mathbf{k}$ and $\mathbf{v}_g$ intersects them at 45°.

The decay rate of a wave has been calculated as a function of θ for each of the three cases, using the results for loss of energy on reflexion given either in Phillips

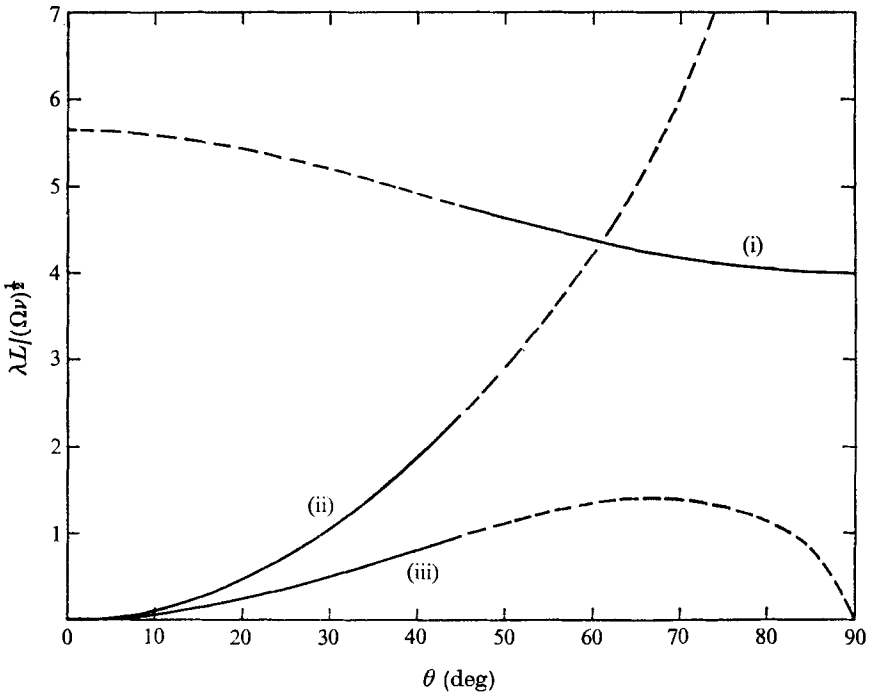

FIGURE 12. The non-dimensional decay rate $\lambda L/(\Omega\nu)^{\frac{1}{2}}$ of reflected inertial waves as a function of θ, the angle between the wavenumber vector **k** and the rotation axis, in three cases: (i) two horizontal reflecting planes; (ii) two vertical reflecting planes, intersected by **Ω**, **k** plane at $\frac{1}{8}\pi$; (iii) two vertical reflecting planes, intersected by **Ω**, **k** plane at $\frac{1}{4}\pi$.

(1963) or by the corresponding theory for (in Phillips' notation†) $\cos\theta < \cos\eta$. The decay rate is defined as

$$\lambda = (1-\sigma)v_{gn}/L \quad (1-\sigma = \epsilon), \tag{26}$$

where σ is (as in Phillips' paper) the ratio of the square of the reflected amplitude to the square of the incident amplitude, and v_{gn} is the component of the group velocity in the direction normal to the reflecting surface. Figure 12 shows $\lambda L/(\Omega\nu)^{\frac{1}{2}}$ as a function of θ for each of the three examples. The dashed portions of the curves are less likely to occur because of the direction of the group velocity: a small-θ wave is more likely to meet vertical walls; a large-θ wave is more likely to meet horizontal walls.

It is seen that typical values of the calculated decay rate are rather smaller than the observed rate for the turbulence. An average value of $\lambda L/(\Omega\nu)^{\frac{1}{2}}$ might perhaps be taken as about 3 compared with the observed decay rates (B and C) of about 7. One still has some difficulty in explaining why the turbulence decays so rapidly.

The above theoretical examples do not allow for a wave being reflected consecutively from both horizontal and vertical boundaries. Such a wave would

† His θ is different from ours.

travel a shorter distance between reflexions and thus decay faster. However, it is doubtful whether this is a large enough effect to explain the differences.

The process of spin-up can be considered as the limiting case of the above wave-reflexion process for $\theta = \frac{1}{2}\pi$. It was seen in §3.4 that the actual spin-up rate was about twice the theoretical value, and this was attributed to the roughness and porosity of the horizontal boundaries. This raises the interesting question of whether the decay of inertial waves is similarly affected by these qualities. Tentatively, this seems the most likely explanation of the discrepancy.

7. Concluding remarks

The principal conclusions reached in previous sections are as follows.

(i) Rotation increases the decay rate of the turbulence. The probable mechanism is the transfer of energy by inertial waves to the boundaries, where it is dissipated in viscous boundary layers.

(ii) The spectral evolution in the rotating turbulence can also be interpreted in terms of this model. Internal viscous dissipation has to be taken into account at higher wavenumbers, but transfer of energy between wavenumbers plays a much more minor role than in the absence of rotation.

(iii) The decays of velocity fluctuations parallel to and perpendicular to the rotation axis apparently remain closely coupled.

(iv) Rotation produces a marked increase in the integral scale parallel to the rotation axis, and a smaller increase in the integral scale perpendicular to the rotation axis. The former can be interpreted as a 'direct Taylor–Proudman effect', the latter as an 'indirect Taylor–Proudman effect' related to the likely properties of two-dimensional turbulence.

The following question arises: what is the relationship between the different ideas invoked to interpret different parts of the data? Since the Taylor–Proudman theorem applies only to steady flow, any interpretation using this theorem involves significant oversimplification, and contains the implication that some unsteady flows exhibit similar properties. This is indeed true of inertial waves of sufficiently low $\omega/2\Omega$. For any particular value of $\omega/2\Omega$ (and thus of θ), one can calculate the ratio of the axial wavenumber to the average wavenumber in any perpendicular direction. By the supposition that the motion is dominated by waves in a certain range of $\omega/2\Omega$, one can thus explain the difference in length scales in different directions. However, this approach also predicts the ratio w'^2/v'^2, which becomes greater than unity in the conditions for which the axial length scale is the larger. Hence, whilst the inertial-wave model can also be said to account for the coupling between the velocity fluctuation components, there is marked quantitative disagreement with the experimental results. It therefore appears that there are limitations to the representation of the turbulence as a random superposition of inertial waves; whilst the dynamical processes associated with inertial waves certainly come into play, aspects of the observations suggest that, even at very low Rossby number, this remains an incomplete description.

The foregoing remarks about length scales relate to the difference in different directions when there is rotation. The fact that both length scales increase more

than in the absence of rotation can not be explained in terms of inertial-wave behaviour, since the magnitude of the wavenumber does not affect this behaviour. This increase is almost certainly a nonlinear effect, presumably occurring at those intermediate times when the Rossby number has become low enough for the rotation to be having a significant influence but not so low that nonlinear effects are entirely negligible. This interpretation is consistent with the observation that the increase occurs up to approximately $t = 10$ s and the length scales then become effectively constant (in so far as one can infer length scales from figure 5). The comments about length scales in §4.4 may have more relevance to this nonlinear regime than do other parts of our interpretation, although these comments are clearly a considerable oversimplification.

The rotating table was designed and its construction supervized by Dr C. W. Titman. Assistance with the design of the mechanical parts of the rest of the apparatus was given by Mr J. Davison, and the constructional work was mainly carried out by Mr J. A. Doss. Financial support for the project was given by the Natural Environment Research Council under research grant GR/3/2395, both for equipment and for the salary of the first author. We are most grateful for this assistance, all of which was essential to the project.

Appendix. Notation

The following list defines symbols used throughout the paper and in the presentation of results. Other symbols used in only one place are defined in the text.

Our notation, where possible, follows that used by Hinze (1959) for turbulence quantities. Thus lower case letters denote fluctuating variables, while upper case letters denote mean or steady variables. Root-mean-square values are denoted by primed symbols, e.g. $v' = (\overline{v^2})^{\frac{1}{2}}$.

(r, ϕ, z)	cylindrical polar co-ordinates fixed in the annulus
(u, v, w)	turbulent velocity fluctuations in the three co-ordinate directions
q'^2	total turbulence kinetic energy ($q'^2 = u'^2 + v'^2 + w'^2$)
$\mathbf{k} = (k_1, k_2, k_3)$	wavenumber (of turbulence or inertial waves), $k = \lvert\mathbf{k}\rvert = 2\pi/$ wavelength
(E_1, E_2, E_3)	one-dimensional energy spectra (with respect to k_2) of (u, v, w) respectively
E	symbol used in general discussion to represent any of (E_1, E_2, E_3)
R_{22}	correlation coefficient of azimuthal velocity fluctuations at two positions
D	depth of annulus
a, $2a$	inner and outer radii of annulus
M	mesh length of grid in annulus (or wind tunnel)
d	grid hole diameter
d'	bar diameter in wind-tunnel grid
Ω	angular rotation rate of annulus
ν	kinematic viscosity of air

v_0', w_0'	initial r.m.s. turbulence intensities in azimuthal and vertical directions
t	time measured from initiation of grid traverse in each run
x	distance downstream from grid in wind tunnel
Δr, Δz	probe separations in radial and vertical directions during correlation measurements
ω	angular frequency
$\mathbf{v}_g$	inertial-wave group velocity
L	size of enclosure in inertial-wave model
θ	angle between wavenumber vector and rotation axis
λ	decay rate of inertial waves
N	Brunt–Väisälä angular frequency

REFERENCES

BAINES, W. D. & PETERSON, E. G. 1951 *Trans. A.S.M.E.* **73**, 467.

BATCHELOR, G. K. 1953 *The Theory of Homogeneous Turbulence*. Cambridge University Press.

BATCHELOR, G. K. 1969 *Phys. Fluids*, **12** (suppl. II), 233.

BATCHELOR, G. K. & TOWNSEND, A. A. 1948*a* *Proc. Roy. Soc.* A **193**, 539.

BATCHELOR, G. K. & TOWNSEND, A. A. 1948*b* *Proc. Roy. Soc.* A **194**, 527.

BRETHERTON, F. P. & TURNER, J. S. 1968 *J. Fluid Mech.* **32**, 449.

COMTE-BELLOT, G. & CORRSIN, S. 1971 *J. Fluid Mech.* **48**, 273.

FJØRTOFT, R. 1953 *Tellus*, **5**, 225.

GOUGH, D. O. & LYNDEN-BELL, D. 1968 *J. Fluid Mech.* **32**, 437.

GREENSPAN, H. P. 1968 *The Theory of Rotating Fluids*. Cambridge University Press.

HINZE, J. O. 1959 *Turbulence*. McGraw-Hill.

HOWARD, L. N. 1969 *Deep-Sea Res.* **16**, 97.

KRAICHNAN, R. H. 1967 *Phys. Fluids*, **10**, 1417.

LING, S. C. & HUANG, T. T. 1970 *Phys. Fluids*, **13**, 2912.

PHILLIPS, O. M. 1963 *Phys. Fluids*, **6**, 513.

SATO, H. 1951 *J. Phys. Soc. Japan*, **6**, 387.

SATO, H. 1952 *J. Phys. Soc. Japan*, **7**, 392.

SCORER, R. S. 1965 *Rep. Dept. Math., Imperial College, London.*

STARR, V. P. 1968 *Physics of Negative Viscosity Phenomena*. McGraw-Hill.

STEWART, R. W. & TOWNSEND, A. A. 1951 *Phil. Trans.* A **243**, 359.

STRITTMATTER, P. A., ILLINGWORTH, G. & FREEMAN, K. C. 1970 *J. Fluid Mech.* **43**, 539.

TOWNSEND, A. A. 1956 *The Structure of Turbulent Shear Flow*. Cambridge University Press.

TRAUGOTT, S. C. 1958 *Nat. Advis. Comm. Aero. Wash., Tech. Note*, no. 4135.

UBEROI, M. S. & WALLIS, S. 1967 *Phys. Fluids*, **10**, 1216.

UBEROI, M. S. & WALLIS, S. 1969 *Phys. Fluids*, **12**, 1355.

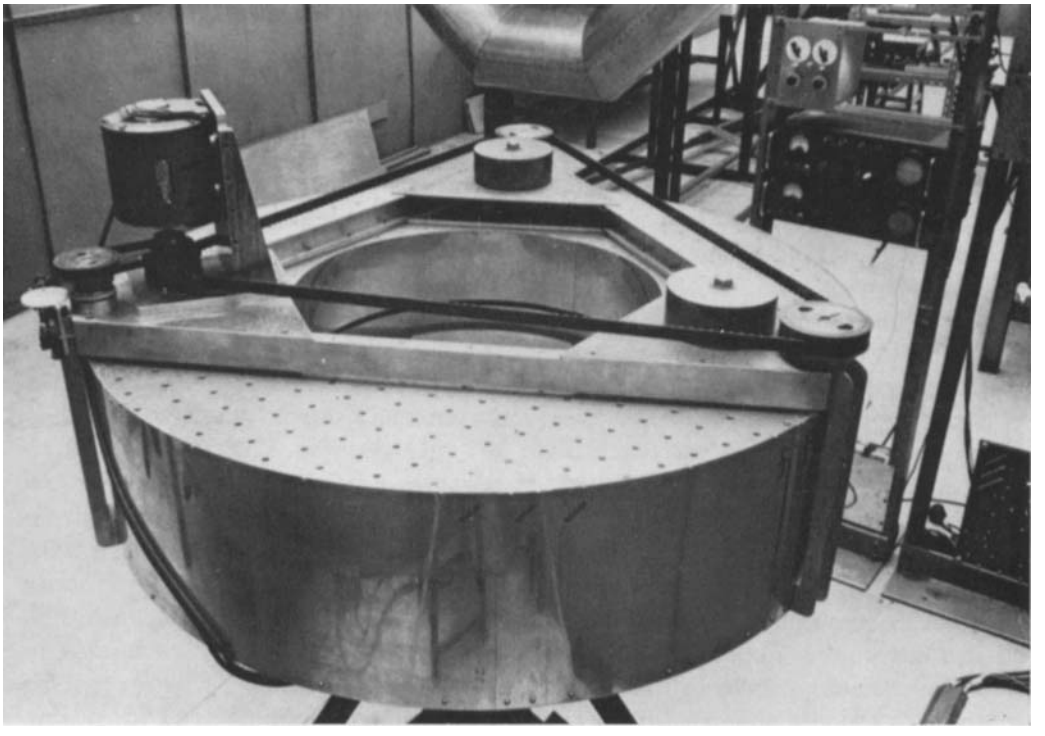

FIGURE 2. Photograph of the apparatus, taken obliquely from above, with the grids in their final positions.